

## **Extended Essay — Physics**

### **Title:**

The Relationship Between Bluff Body Geometry and Vortex Shedding Frequency in a  
Two-Dimensional Laminar Flow

### **RQ:**

How does increasing the number of streamwise faces of a bluff body (ranging from 2 to 12) affect the vortex shedding frequency in laminar flow, measured in Hz, in a two-dimensional plane?

Word count:

3994

Examination Session: **May 2026**

# Contents

<b>1</b>	<b>Introduction</b>	<b>6</b>
<b>2</b>	<b>Background</b>	<b>7</b>
2.1	Frequency and Time Period . . . . .	7
2.2	Fundamentals of Fluid Dynamics . . . . .	7
2.3	Vortex Shedding and the Kármán Vortex Street . . . . .	9
2.4	The Mechanism of Vortex Shedding . . . . .	9
2.5	Hypothesis . . . . .	12
<b>3</b>	<b>Variables</b>	<b>13</b>
3.1	Constant Variables of Theoretical Investigation . . . . .	13
3.2	Constant Variables of Practical Investigation . . . . .	14
<b>4</b>	<b>Equipment</b>	<b>15</b>
<b>5</b>	<b>Method</b>	<b>17</b>
5.1	The Bluff Body . . . . .	17
5.2	The Theoretical Investigation . . . . .	18
5.2.1	Ansys Workbench . . . . .	18
5.2.2	The OpenFOAM Simulation . . . . .	20
5.2.3	Simulation Settings . . . . .	20
5.3	The Practical Investigation . . . . .	24
5.4	Determining the vortex shedding frequency . . . . .	28
5.4.1	Theoretical Investigation . . . . .	29
5.4.2	Practical Investigation . . . . .	29
<b>6</b>	<b>Results</b>	<b>30</b>
6.1	Raw Data of the Theoretical Investigation . . . . .	30
6.1.1	Sample Table of Time vs. Lift Coefficient ( $C_L$ ) for Bluff Body $n = 2$ .	30
6.2	Processed Data of the Theoretical Investigation . . . . .	32

6.2.1	Representative (Average) Lift Coefficient ( $C_L$ ) Over Time for Each Bluff Body	32
6.2.2	Sample Calculation of Vortex Shedding Frequency for Bluff Body $n = 2$ using Python	38
6.2.3	A Comparison of Vortex Shedding Frequency with Increasing $n$ from 2 – 12	39
6.3	Results of Practical Investigation	41
<b>7</b>	<b>Conclusion</b>	<b>42</b>
<b>8</b>	<b>Evaluation</b>	<b>44</b>
8.1	Evaluation of the Theoretical Investigation	44
8.2	Evaluation of the Practical Investigation	45
<b>Appendices</b>		<b>51</b>
<b>A</b>	<b>Python Code</b>	<b>51</b>
<b>B</b>	<b>Snapshots of Practical Investigation</b>	<b>54</b>

# List of Figures

1	Von Kármán Street behind a cylinder in a non-rotating 2D flow for $Re = 140$ , fluorescein visualization (Ilieva, 2017, p. 144). . . . .	9
2	Depiction of boundary layer and the velocity gradient formed. The red dotted line depicts the outline of the boundary layer. Inspired by Embry-Riddle Aero-nautical University (n.d.). . . . .	10
3	The mechanism of vortex shedding. Inspired by Shen et al. (2010, p. 3). . . . .	11
4	Examples of the top view of the bluff bodies. . . . .	17
5	The fluid domain with dimensions. Example with bluff body $n = 2$ . Inspired by comflics (2014). . . . .	18
6	The fluid domain with dimensions and the BOI. Example with bluff body $n = 2$ . Inspired by comflics (2014). . . . .	19
7	Example of mesh of fluid domain with bluff body $n = 2$ . Visualized in ParaView. .	20
8	Overview of the simulation directory structure. Modified files are highlighted blue. Created files and folders are highlighted green. . . . .	21
9	The setup for the practical investigation (angle 1). . . . .	24
10	The setup for the practical investigation (angle 2). . . . .	25
11	A bluff body positioned in the flow tank with potassium permanganate crystals spread in front of it. . . . .	26
12	The 3D-printed bluff bodies of fixed height. The numbers correspond to the number of inlet-facing sides. . . . .	27
13	Average lift coefficient $C_L$ over time for the bluff body $n = 2$ , based on identical simulation results. The red dashed line indicates the start of periodic vortex shedding at $t = 1$ s. . . . .	32
14	Average lift coefficient $C_L$ over time for the bluff body $n = 3$ , based on identical simulation results. The red dashed line indicates the start of periodic vortex shedding at $t = 1$ s. . . . .	32

15	Average lift coefficient $C_L$ over time for the bluff body $n = 4$ , based on identical simulation results. The red dashed line indicates the start of periodic vortex shedding at $t = 1$ s. . . . .	33
16	Average lift coefficient $C_L$ over time for the bluff body $n = 5$ , based on identical simulation results. The red dashed line indicates the start of periodic vortex shedding at $t = 1$ s. . . . .	33
17	Average lift coefficient $C_L$ over time for the bluff body $n = 6$ , based on identical simulation results. The red dashed line indicates the start of periodic vortex shedding at $t = 1$ s. . . . .	34
18	Average lift coefficient $C_L$ over time for the bluff body $n = 7$ , based on identical simulation results. The red dashed line indicates the start of periodic vortex shedding at $t = 1$ s. . . . .	34
19	Average lift coefficient $C_L$ over time for the bluff body $n = 8$ , based on identical simulation results. The red dashed line indicates the start of periodic vortex shedding at $t = 1$ s. . . . .	35
20	Average lift coefficient $C_L$ over time for the bluff body $n = 9$ , based on identical simulation results. The red dashed line indicates the start of periodic vortex shedding at $t = 1$ s. . . . .	35
21	Average lift coefficient $C_L$ over time for the bluff body $n = 10$ , based on identical simulation results. The red dashed line indicates the start of periodic vortex shedding at $t = 1$ s. . . . .	36
22	Average lift coefficient $C_L$ over time for the bluff body $n = 11$ , based on identical simulation results. The red dashed line indicates the start of periodic vortex shedding at $t = 1$ s. . . . .	36
23	Average lift coefficient $C_L$ over time for the bluff body $n = 12$ , based on identical simulation results. The red dashed line indicates the start of periodic vortex shedding at $t = 1$ s. . . . .	37

24	Sample visualization of the peaks and troughs identification on the Lift Coefficient $C_L$ over time graph for bluff body $n = 2$ . The initial startup phase, colored in gray, is excluded from the detection. . . . .	38
25	A comparison of vortex shedding frequency with increasing $n$ from 2 – 12. . .	40

# 1 Introduction

Over the past century, vortex shedding has garnered a multifold of attention, with hundreds of papers published (Buresti, 1998, p. 61). This partially elucidated phenomenon is quintessential in a broad range of scientific and engineering contexts, from maintaining ubiquitous infrastructure to developing cutting-edge aerospace technologies. Bridges may suffer from vortex shedding excitation, a severe challenge which undermines their structural integrity (Jurado et al., 2012, p. 1040). This was exemplified by the 1940 collapse of the Tacoma Narrows Bridge, where vortex shedding instigated vertical vibration that eventually transitioned into the torsional oscillations, ultimately causing its collapse (Song et al., 2022).

A profound youthful interest in planes inspired the topic of this essay: vortex shedding. Specifically, this investigation will concern itself with the question: **How does increasing the number of streamwise faces of a bluff body (ranging from 2 to 12) affect the vortex shedding frequency in laminar flow, measured in Hz, in a two-dimensional plane?**

Links can be made to Section C of the IB Physics Guide: *Wave Behavior* (“IB Physics Guide 2025”, 2023). Section C.1, *Simple Harmonic Motion*, concerns itself with an idealized theoretical representation of the behavior of oscillatory systems (Allum & Morris, 2023, p. 313). Fundamental concepts such as frequency and time period are discussed, ideas required in order to analyze the frequency of the vortex shedding caused by a bluff body. Furthermore, the topic of this essay also links to Section C.4, *Standing Waves and Resonance*. Concepts of natural frequency, vibrations and resonance are key when discussing the problems caused by vortex shedding.

## 2 Background

### 2.1 Frequency and Time Period

**Frequency** and **Time period** stand in an inverse relationship

$$f = \frac{1}{T} \quad (1)$$

where  $f$  is frequency in Hz and  $T$  is time period (s). This relationship is later utilized to extrapolate the vortex shedding frequency.

### 2.2 Fundamentals of Fluid Dynamics

**Vorticity** is the vector quantity representing the rotational motion in a velocity field (Holton, 2003, p. 2500). A **vortex** is the circular flow of a fluid around a central axis, characterized by the vorticity in the fluid (Nitsche, 2006, p. 390). A **bluff body** is defined as an object that, due to its geometry, induces significant regions of separated flow (National Research Council, 1997, p. 561).

A **Newtonian fluid** is a fluid in which the viscosity — a measure of internal friction — remains constant despite applied force (Mohn, 2024).

**Laminar flow** is characterized by the layered motion of fluid particles, with no significant disturbance between the parallel layers (Versteeg & Malalasekera, 2007, pp. 40–41). On the other hand, **turbulent flow** is known to have continuous, irregular fluctuations in velocity and pressure throughout the fluid (Versteeg & Malalasekera, 2007, p. 40). In an **incompressible flow** the fluid has a constant density (Versteeg & Malalasekera, 2007, p. 12).

The **Reynolds number** expresses the “ratio between inertial and viscous forces” (NASA Glenn Research Center, 2021). Given by the equation

$$\text{Re} = \frac{UL}{\nu} \quad (2)$$

where  $U$  is the free-stream velocity ( $\text{m s}^{-1}$ ),  $L$  is the characteristic length (m), and  $\nu$  is the kine-

matic viscosity ( $\text{m}^2 \text{s}^{-1}$ ) (“The Relationship Between Reynolds Number and Kinematic Viscosity”, n.d.). Low Reynolds numbers signify laminar flow, while high Reynolds numbers indicate turbulent flow, though the exact threshold values vary between sources (Saldana et al., 2024).

The **Strouhal number** is a dimensionless parameter used to describe the periodicity of vortex shedding (Choi & Kwon, 2000, p. 211). It is given by the equation

$$\text{St} = \frac{fL}{U} \quad (3)$$

where  $f$  is the frequency of vortex shedding (Hz),  $L$  is the characteristic length (m), and  $U$  is the free-stream velocity ( $\text{m s}^{-1}$ ). A high Strouhal number — assuming both  $L$  and  $U$  remain constant — indicates an increased  $f$ , conversely a low Strouhal number indicates a lower  $f$ . The geometry of the bluff body impacts the Strouhal number, and therefore the vortex shedding frequency (Ibrahim, 2022, p. 32). As the theory underlying the geometry-Strouhal relation exceeds this essay’s scope, the hypothesis and analysis rely on the empirical findings of Gonçalves and Del Rio Vieira (1999) that a greater number of streamwise faces decreases the Strouhal number.

Gonçalves and Del Rio Vieira (1999)

This essay will analyze vortex shedding in a Newtonian fluid — water — which exhibits laminar and incompressible flow. A Reynolds number of 100, below reported transitional thresholds, was targeted in order to ensure laminar flow with periodic vortex shedding (Alammar, n.d. p. 2); however, due to practical limitations, this was only fully realized theoretically and not in practice. Given the very limited research in three-dimensional vortex shedding (Buresti, 1998, p. 63), this paper concerns itself with vortex shedding in two dimensions. While the simulation was conducted in a two-dimensional domain, the practical experiment could only approximate two-dimensional flow.

## 2.3 Vortex Shedding and the Kármán Vortex Street

Vortex shedding in a two-dimensional plane can be defined as the phenomenon in which localized regions of high vorticity are periodically released into the wake from alternating sides of a bluff body, each exhibiting an opposite rotational direction (Green, 1995, p. 156). The Kármán Vortex Street refers to the distinct flow pattern created, a repeated structure of counter-rotating vortices (Govardhan & Ramesh, 2005, p. 26).



**Figure 1:** Von Kármán Street behind a cylinder in a non-rotating 2D flow for  $Re = 140$ , fluorescein visualization (Ilieva, 2017, p. 144).

## 2.4 The Mechanism of Vortex Shedding

Due to the friction between a given fluid and a bluff body, there is no relative motion between them (Jeff Defoe, 2020; TutorialsPoint, 2018). Consequently, if the velocity of the bluff body is zero, the velocity of the fluid at the wall of the bluff body, with respect to the reference frame of the bluff body, is also zero: a no-slip condition. This causes a variation in velocities with distance, from zero at the bluff body surface to the free stream velocity  $U$  at a certain distance from the bluff body. The region in which this velocity gradient occurs is referred to as the boundary layer.

Distance

from

bluff body,

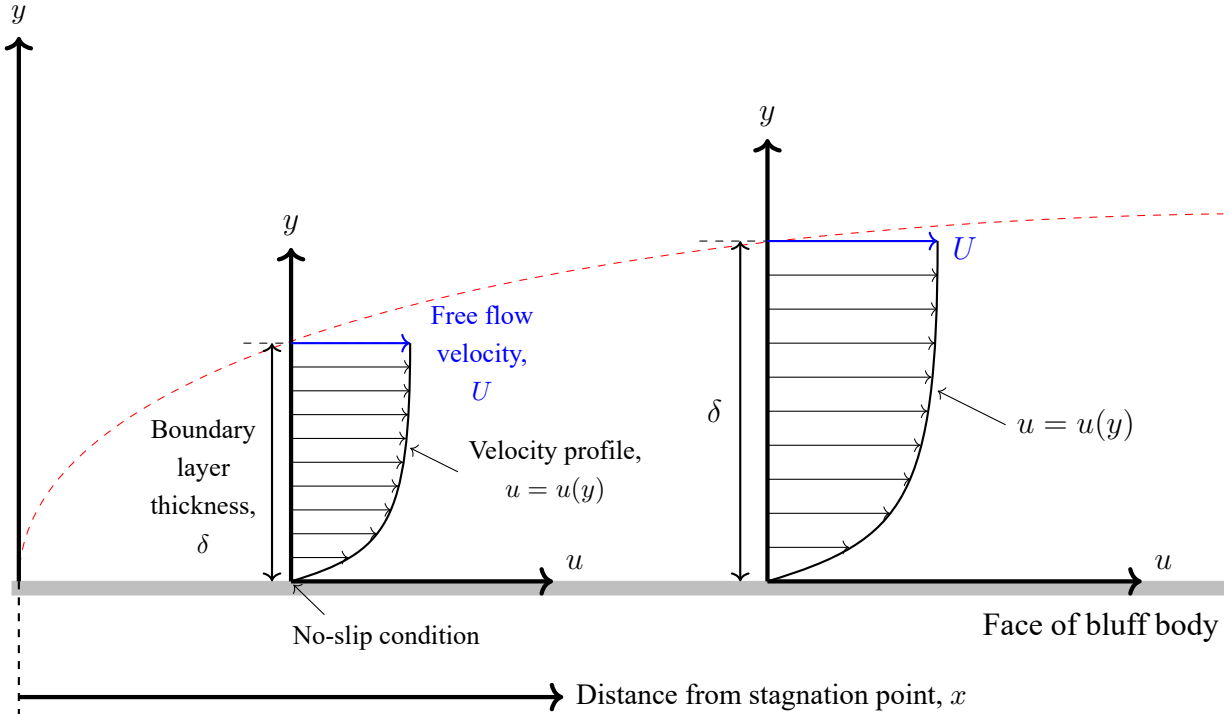


**Figure 2:** Depiction of boundary layer and the velocity gradient formed. The red dotted line depicts the outline of the boundary layer. Inspired by Embry-Riddle Aeronautical University (n.d.).

When a flow moves past a bluff body in a two-dimensional plane, a boundary layer develops, with increasing thickness  $\delta$  from the *stagnation point* (Fitzpatrick, 2016) — the point on the leading edge of the bluff body at which the local fluid velocity is zero (with respect to the bluff body) — to the back of the bluff body (Learn Engineering, 2022).

At a certain point, the boundary layer separates from the bluff body, forming a shear layer. Under steady flow conditions, this separation occurs in a periodic and alternating manner, creating two separate, out-of-phase shear layers on either side of the bluff body.

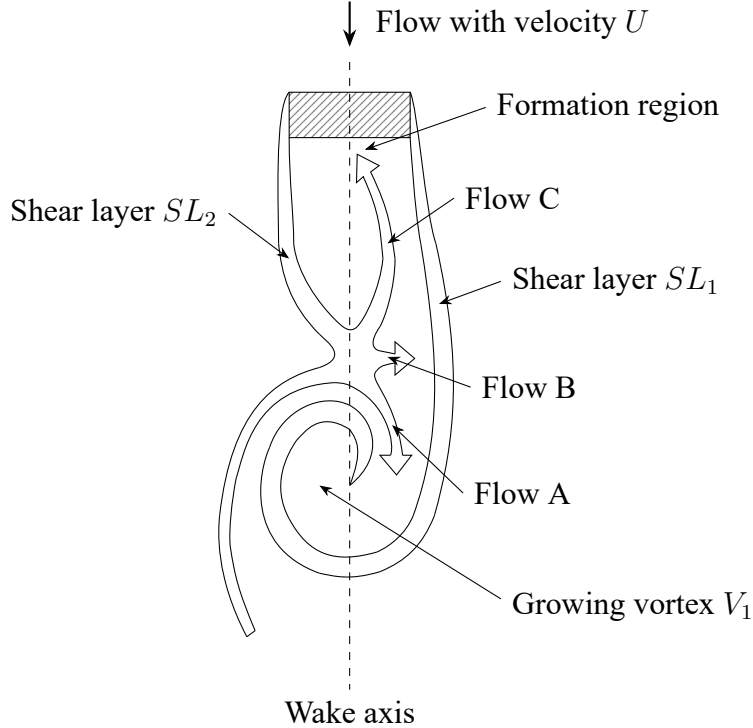


**Figure 3:** The mechanism of vortex shedding. Inspired by Shen et al. (2010, p. 3).

For simplification, assume the first shear layer is generated at the right of the bluff body ( $SL_1$ ). Due to its vorticity, the shear layer tends to curl up, forming a vortex. As the vortex forms, the pressure in the core of the vortex decreases, acting as a sink, inducing inflow towards its center. The fluid initially present at the backside of the bluff body is drawn into the vortex, creating space, allowing for the formation of the left shear layer ( $SL_2$ ) in the *formation region*. This newly created shear layer splits into three distinct flows: a flow (*Flow C*) which recirculates behind the bluff body, a flow (*Flow B*) which mixes with the right shear layer ( $SL_1$ ) and a flow (*Flow A*) which is drawn into the vortex ( $V_1$ ).

There is a decrease in strength of the vortex being created due to *Flow A* having an opposite vorticity to the vorticity of the vortex. Moreover, the opposite vorticity of *Flow B* and the right shear layer effectively nullifies each other, leading to the right shear layer being interrupted and the vortex becoming detached, causing it to travel with the main flow. The vortex has been “shed”. Since the vortex moves away from the bluff body, its low-pressure influence on the area near the bluff body decreases, allowing the left shear layer to develop more freely. Now, due to the periodic nature of vortex formation, the process recurs with the shear layers switching roles.

When considering the vortex being created from the right shear layer ( $SL_1$ ), the fluid on the right of the vortex will have the same velocity as the free stream velocity  $U$ , whereas the velocity on the left of the vortex will be of a smaller magnitude and in the opposite direction of the main flow. According to Bernoulli's equation, a region of higher velocity must have a lower pressure and vice versa. Therefore, the left region of the vortex will have a higher pressure than the right region, causing a lift force which acts on the bluff body normal to the flow. The oscillation of this lift force coincides with the vortex shedding frequency  $f$ .

## 2.5 Hypothesis

As the number of streamwise faces of the bluff body increases from 2 to 12, the vortex shedding frequency in laminar flow will decrease. Confirmed by Gonçalves and Del Rio Vieira (1999), this trend is attributed to a decrease in the Strouhal number as the number of streamwise faces increase, which is directly proportional to the vortex shedding frequency (see Equation (3)).

## 3 Variables

**Independent Variable:** Number of streamwise faces  $n$  of the bluff body (ranging from 2 to 12)

•

**Dependent Variable:** The vortex shedding frequency (Hz) (see Section 5.4)

### 3.1 Constant Variables of Theoretical Investigation

Constant Variables	How it is kept constant	Justification
Overall length of bluff body i.e. the characteristic length (m)	The bluff bodies were constructed in Ansys Workbench with identical overall lengths	Impacts the Strouhal number and in turn the vortex shedding frequency (see Equation (3))
Simulation settings	Identical simulation settings were used for each trial	Various parameters could impact the vortex shedding frequency outside the intended variation due to the independent variable (detailed in Section 5.2.3)
Fluid domain dimensions (m)	The fluid domains were established with the same dimensions	Impacts the development of the flow and therefore the vortex shedding frequency
Mesh resolution (m)	The meshes were made using identical parameters	Standardizes numerical uncertainties across all trials (Przulj, 1998)

### 3.2 Constant Variables of Practical Investigation

Constant Variables	How it is kept constant	Justification
Overall length of bluff body i.e. the characteristic length (m)	Bluff bodies constructed and 3D-printed with equal overall lengths	Impacts the Strouhal number and in turn the vortex shedding frequency (see Equation (3))
Fluid used (water)	Flow tank filled with water	Different fluids have varied kinematic viscosities, altering the Reynolds number
Water temperature (°C)	The trials were conducted in one setting with constant room temperature	Temperature impacts kinematic viscosities, altering the Reynolds number (“The Relationship Between Reynolds Number and Kinematic Viscosity”, n.d.)
Flow velocity ( $\text{m s}^{-1}$ )	The setting of the water pump and regulation value were kept constant	Flow velocity impacts the Reynolds number which should be kept constant to ensure identical flow conditions
Material and surface finish of bluff bodies	The bodies were 3D-printed utilizing the same material	Material inconsistencies disrupt the flow, impacting the vortex shedding frequency
Measurement duration (min)	Each bluff body was recorded for an equal duration	Ensuring consistency when determining the vortex shedding frequency
Lighting conditions Camera setup and lighting conditions	Camera settings and the lamp positioning and brightness remain unchanged	The vortices are equally identifiable

## 4 Equipment

Theoretical Investigation	Practical Investigation
<ul style="list-style-type: none"> <li>– Ansys Workbench (“Ansys Workbench   Simulation Integration Platform”, n.d.)</li> <li>– Windows Subsystem for Linux (WSL) (“Windows Subsystem for Linux (WSL)”, n.d.)</li> <li>– OpenFOAM (“OpenFOAM”, 2024)</li> <li>– ParaView (“ParaView - Open-source, multi-platform data analysis and visualization application”, n.d.)</li> <li>– Python (“Welcome to Python.org”, 2025)</li> </ul>	<ul style="list-style-type: none"> <li>– Original Prusa MINI 3D Printer with PLA filament (“Original Prusa MINI+ Halbmontiert   Original Prusa 3D-Drucker direkt von Josef Prusa”, n.d.)</li> <li>– Slicer for Prusa MINI 3D Printer (“PrusaSlicer   Original Prusa 3D-Drucker direkt von Josef Prusa”, n.d.)</li> <li>– FreeCAD (“FreeCAD”, n.d.)</li> <li>– Aquarium of size 1.18 m × 0.32 m × 0.44 m</li> <li>– 75 W Water pump (“Lnicez Schmutzwasser-Tauchpumpe(75 W, Ø19 mm,3.000L/H)”, n.d.)</li> <li>– Waterproof liquid glue</li> <li>– Saw</li> <li>– Piping with diameter <math>\varnothing 0.017</math> m</li> <li>– Pipe corner pieces with diameter <math>\varnothing 0.017</math> m</li> <li>– Regulation valve</li> </ul>

**Table 1:** A list of the equipment required for both the theoretical and practical investigation.

Theoretical Investigation	Practical Investigation
	<ul style="list-style-type: none"> <li>– Hose clamp</li> <li>– Hose connecting to water supply</li> <li>– Water supply</li> <li>– GoPro</li> <li>– Knife</li> <li>– Potassium permanganate crystals</li> <li>– Spatula</li> <li>– Permanent Marker</li> <li>– Digital stopwatch</li> <li>– Goggles</li> <li>– Gloves</li> <li>– Waste tank</li> <li>– Float</li> </ul>

**Table 2 (continued):** A list of the equipment required for both the theoretical and practical investigation.

## 5 Method

### 5.1 The Bluff Body

In order to maintain a cylinder-like appearance, one of the most common bluff bodies investigated (Rocchi & Zasso, 2002, p. 475), this investigation used bluff bodies featuring a rectangular “tail”. This results in each bluff body having an overall length  $\ell$  in both streamwise and transverse directions — analogous to a cylinder. The characteristic length  $L$  of each bluff body is therefore equal to the overall length  $\ell$ . Bluff bodies with streamwise faces  $n$  ranging from 2 to 12 were investigated. The lengths of the  $n$  faces within the bluff body  $n$  were homogeneous. A square bluff body ( $n = 1$ ) was excluded due to its fundamentally different flow interaction attributed to the lack of multiple streamwise faces. As the practical investigation occurs in three dimensions, each bluff body was constructed with a fixed height, approximating the two-dimensional behavior observed in the simulation (see Figure 12).

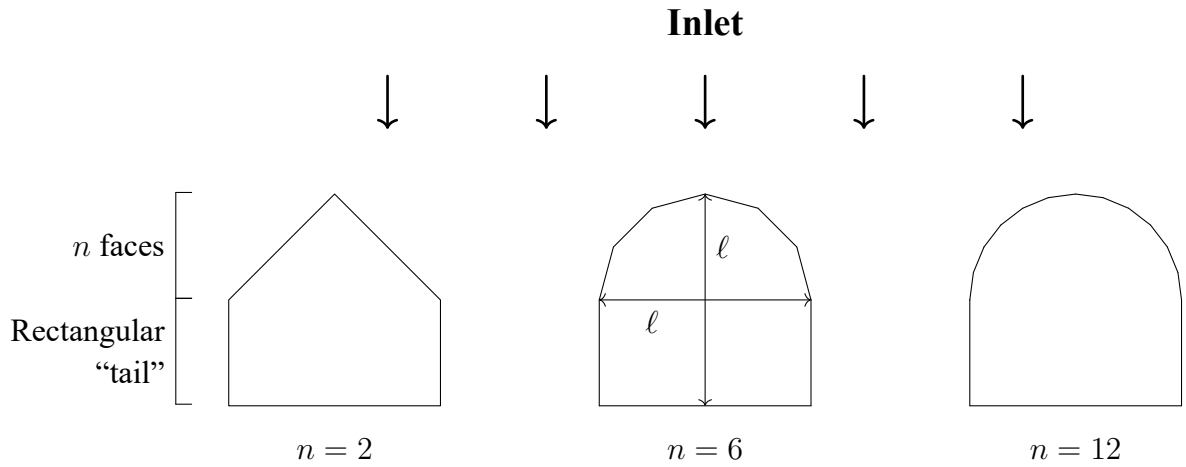


**Figure 4:** Examples of the top view of the bluff bodies.

## 5.2 The Theoretical Investigation

### 5.2.1 Ansys Workbench

The geometry and mesh preparation for the simulation was conducted using Ansys Workbench (“Ansys Workbench | Simulation Integration Platform”, n.d.). The dimensions of the fluid domain are based on Figure 5 where  $\ell$  is the overall length of the bluff body.

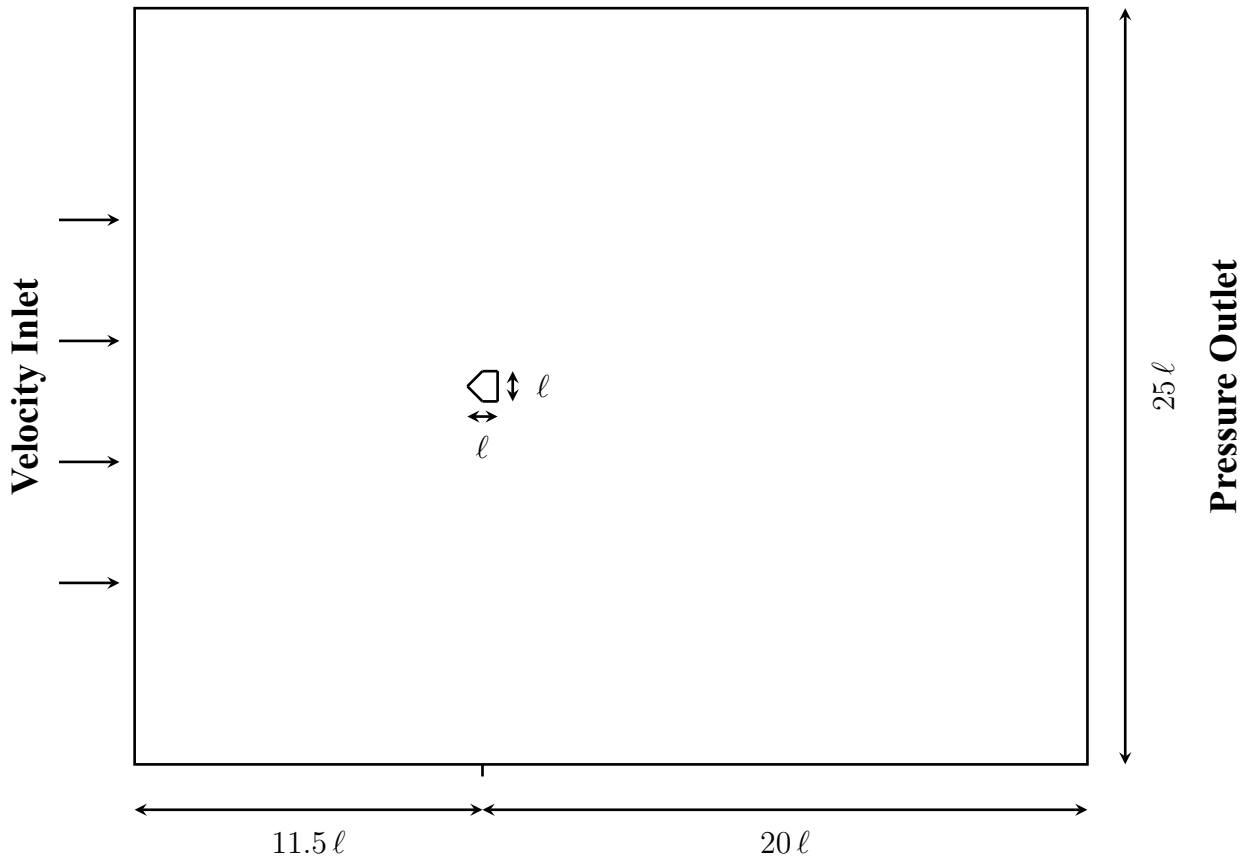


**Figure 5:** The fluid domain with dimensions. Example with bluff body  $n = 2$ . Inspired by comflics (2014).

Given the computational limitations of the computer the simulation was conducted on,  $\ell = 1 \times 10^{-3}$  m was chosen — therefore  $L = 1 \times 10^{-3}$  m.

The *All Triangles Method* was utilized to create the mesh. A global unit size of  $2.25 \times 10^{-3}$  m was applied to the fluid domain to ensure a computationally inexpensive resolution in regions of negligible interest. Conversely, near the edge of the bluff body, a significantly smaller unit size of  $2.0 \times 10^{-5}$  m was used, constituting an accurate depiction of the interaction between the

fluid flow and the bluff body (Ansys Learning, 2023). Furthermore, eight inflation layers were employed in order to precisely capture the gradients associated with boundary layer formation at the edges of the bluff body (Fluid Mechanics 101, 2021). Moreover, a body of influence (BOI) with a sizing of  $2.0 \times 10^{-4}$  m was used — positioned as shown in Figure 6 — refining the mesh around the bluff body and also in the wake region (where the vortex shedding occurs), constituting for a more exact simulation.

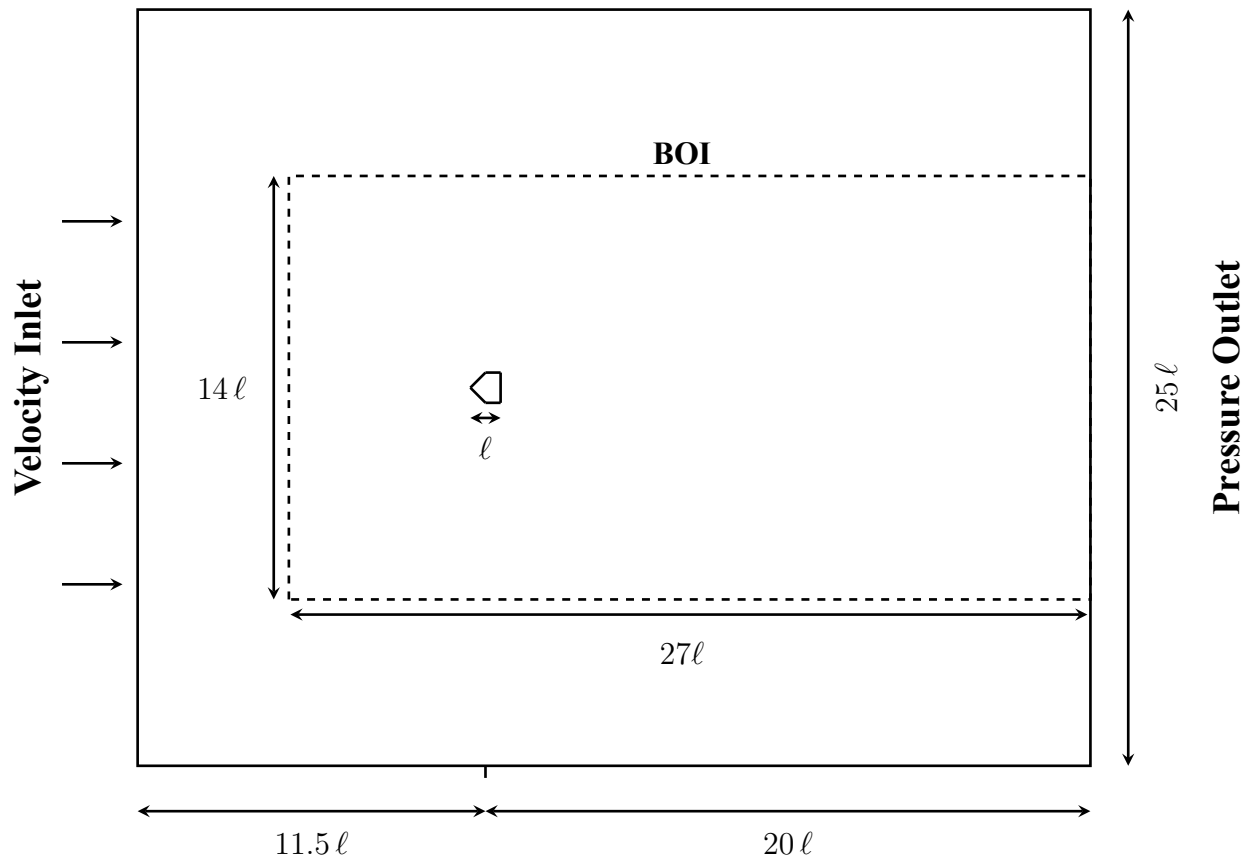


**Figure 6:** The fluid domain with dimensions and the BOI. Example with bluff body  $n = 2$ . Inspired by comflics (2014).

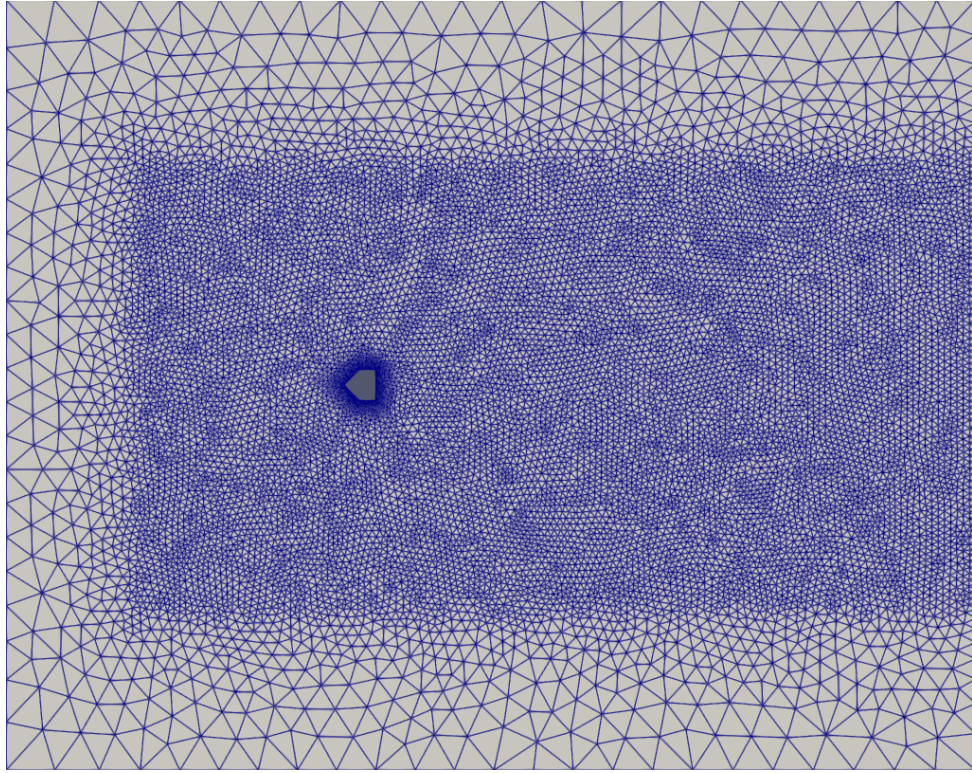


**Figure 7:** Example of mesh of fluid domain with bluff body  $n = 2$ . Visualized in ParaView.

### 5.2.2 The OpenFOAM Simulation

The theoretical part of this EE was conducted using the open-source CFD software package OpenFOAM (“OpenFOAM”, 2024) in Windows Subsystem for Linux (WSL) (“Windows Subsystem for Linux (WSL)”, n.d.). The solver pimpleFOAM was chosen as it facilitates robust handling of both laminar and turbulent flow, enabling the verification if the flow is truly laminar (“pimpleFoam - OpenFOAM Solver - SimFlow CFD Software”, n.d.). Utilizing reporting functions, one can extract the lift coefficient  $C_L$ , which shows the fluctuations in the lift force acting on the bluff body.

### 5.2.3 Simulation Settings

To adhere to the scope of this essay, the simulation setup was adapted from a case study provided in the Udemy course *OpenFOAM for Absolute Beginners* by Jayaraj P (2024). The tutorial case *3vortexShedding*, discussed in lecture eight, served as a structural template and was modified to align with the specific requirements of this investigation.

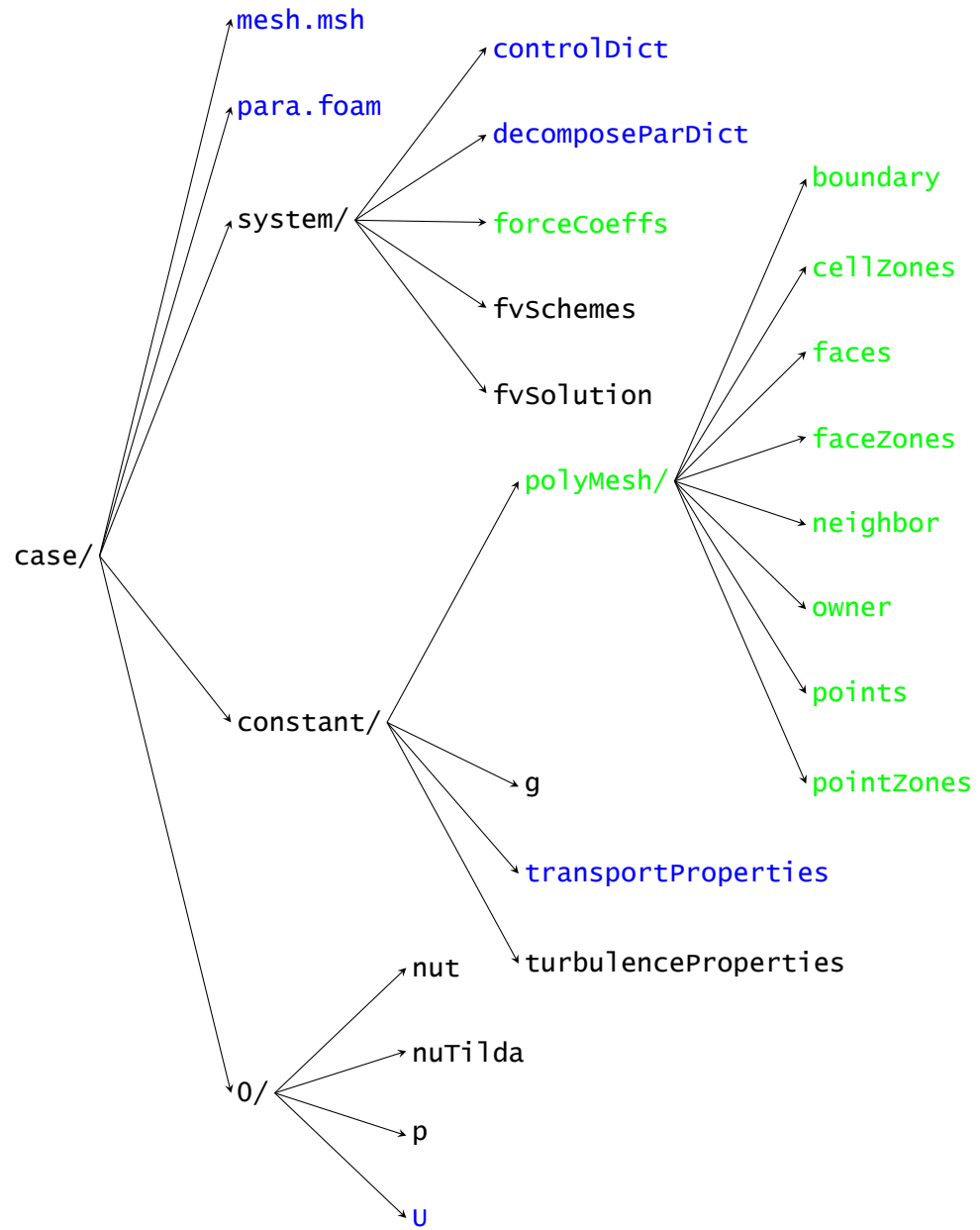


**Figure 8:** Overview of the simulation directory structure. Modified files are highlighted blue. Created files and folders are highlighted green.

File	Parameter	Original	Modified	Justification
mesh.msh, para.foam, polyMesh/ boundary cellZones faces faceZones neighbor owner points pointsZones	—	mesh.msh defines, polyMesh/ contains and para.foam visualizes the mesh of fluid domain of tuto- rial case	mesh.msh defines, polyMesh/ contains and para.foam visualizes the mesh of fluid domain with dimensions given in Section 5.2.1	The fluid domain was adjusted to conform with the computational limits discussed in Section 5.2.1, while achieving the Reynolds number required for this investigation
controlDict	deltaT	0.0002	0.00001	Decreased in order to achieve a greater accuracy (Versteeg & Malalasekera, 2007, p. 289) while ensuring numerical stability (Caminha, 2017).
	functions	none	#include "forceCoeffs"	Reporting function, defined in forceCoeffs, included in order to extract the lift coefficient $C_L$ (Codeynamics, 2024)
	adjustTimeStep	yes	no	Removed as the simulation demonstrated stable behavior with the adjusted deltaT (Jayaraj P, 2024)

**Table 2:** Overview of the changes made to the simulation template.

File	Parameter	Original	Modified	Justification
decomposeParDict	numberofsubdomains	8	6	The simulations were performed on a system with 6 processing cores (Jayaraj P, 2024)
forceCoeffs	—	—	Created a reporting function which outputs the variation of the lift coefficient $C_L$ throughout the simulation	Lift coefficient $C_L$ is needed for subsequent calculation of vortex shedding frequency $f$
transportProperties	nu	$1 \times 10^5$	$1 \times 10^6$	The kinematic viscosity of water at 20°C is approximately $1 \times 10^6 \text{ m}^2 \text{ s}^{-1}$ (“Water - Dynamic and Kinematic Viscosity at Various Temperatures and Pressures”, n.d.)
U	inlet value (x, y, z)	x = 10	x = 0.1	Adapted in order to achieve the target Reynolds number of 100 using Equation (2) where $L = 1 \times 10^{-3} \text{ m}$ , $\nu = 1 \times 10^{-6} \text{ m}^2 \text{ s}^{-1}$ and $U = 0.1 \text{ m s}^{-1}$

**Table 3 (continued):** Overview of the changes made to the simulation template.

### 5.3 The Practical Investigation

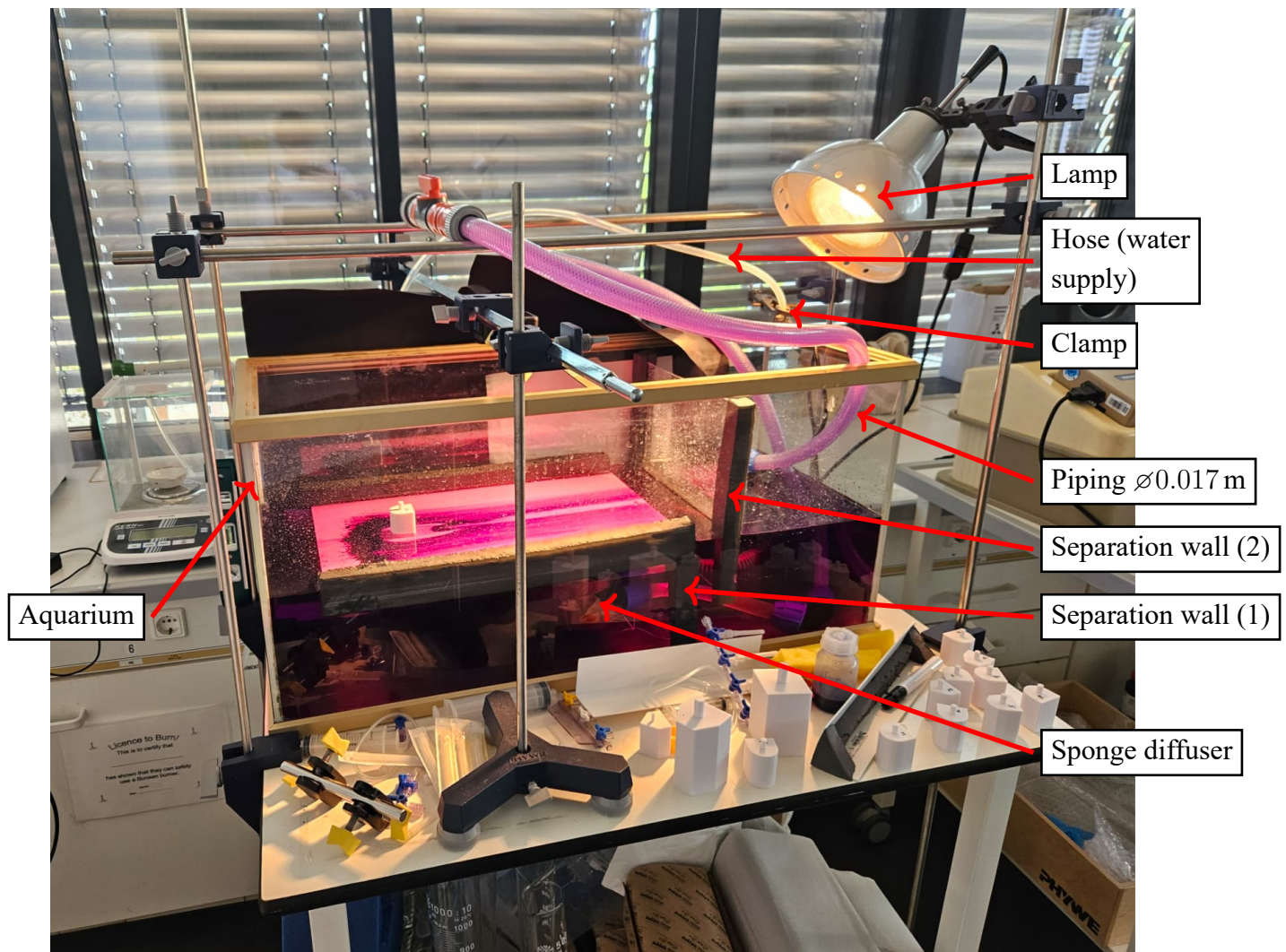


**Figure 9:** The setup for the practical investigation (angle 1).

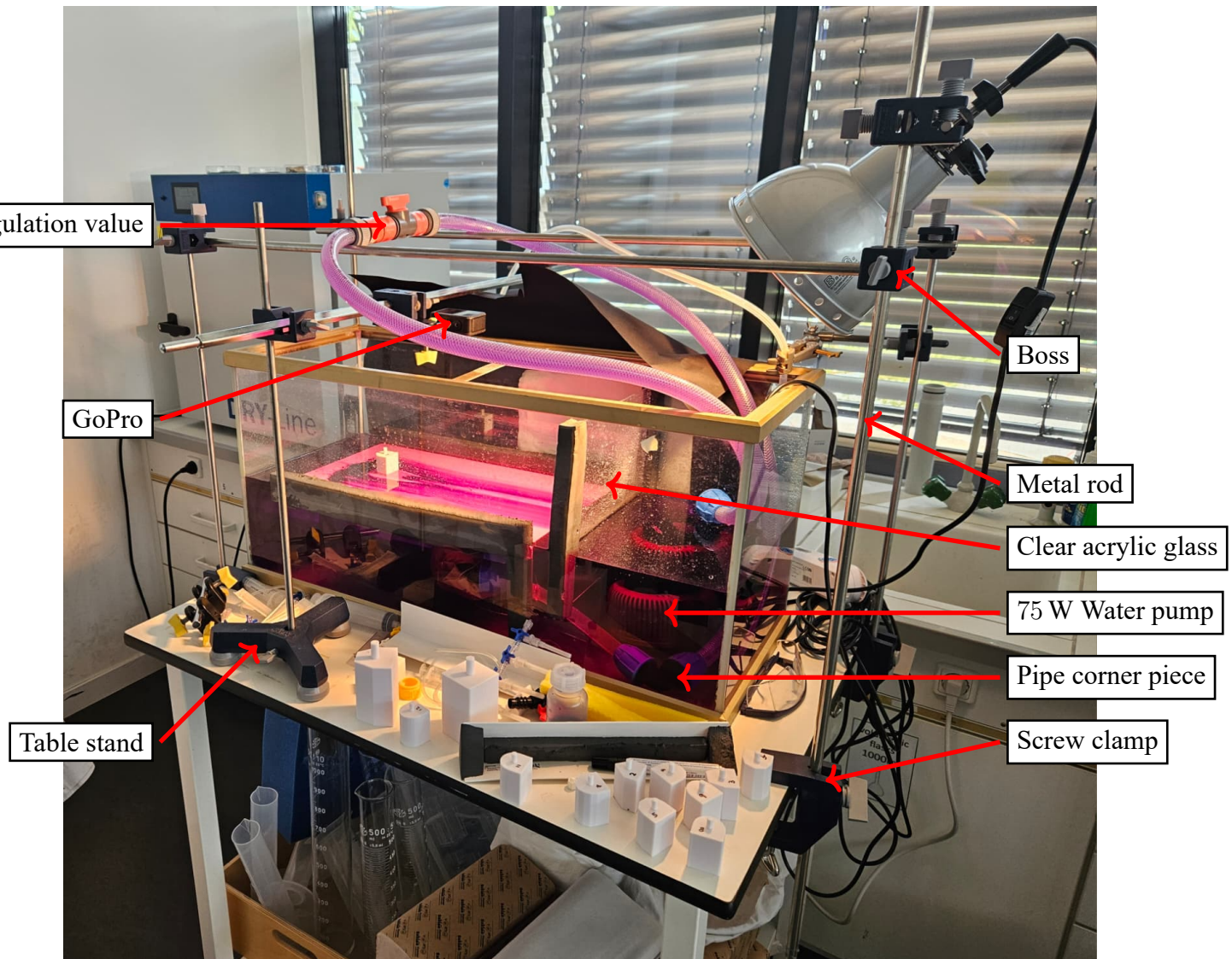


**Figure 10:** The setup for the practical investigation (angle 2).

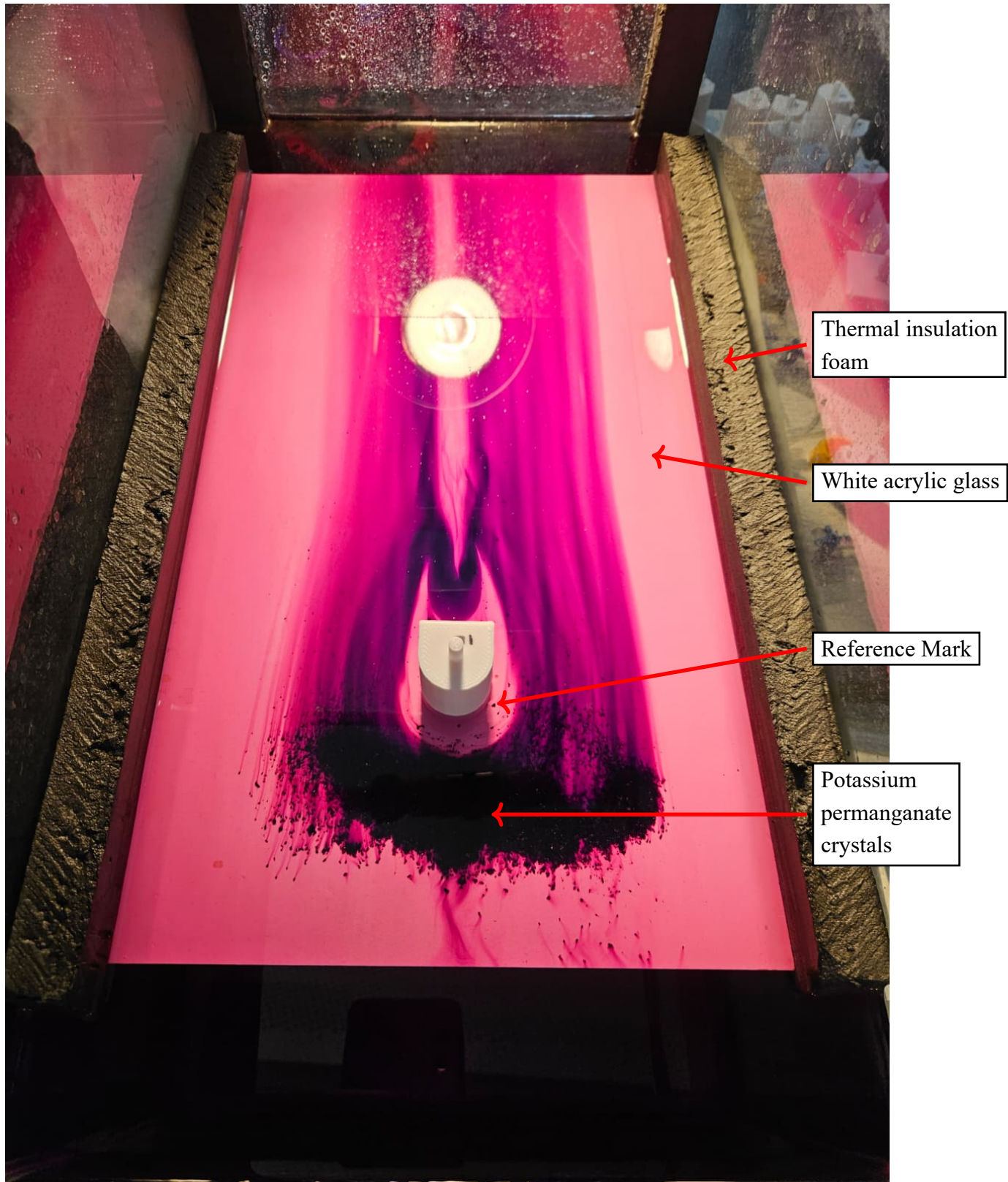


**Figure 11:** A bluff body positioned in the flow tank with potassium permanganate crystals spread in front of it.

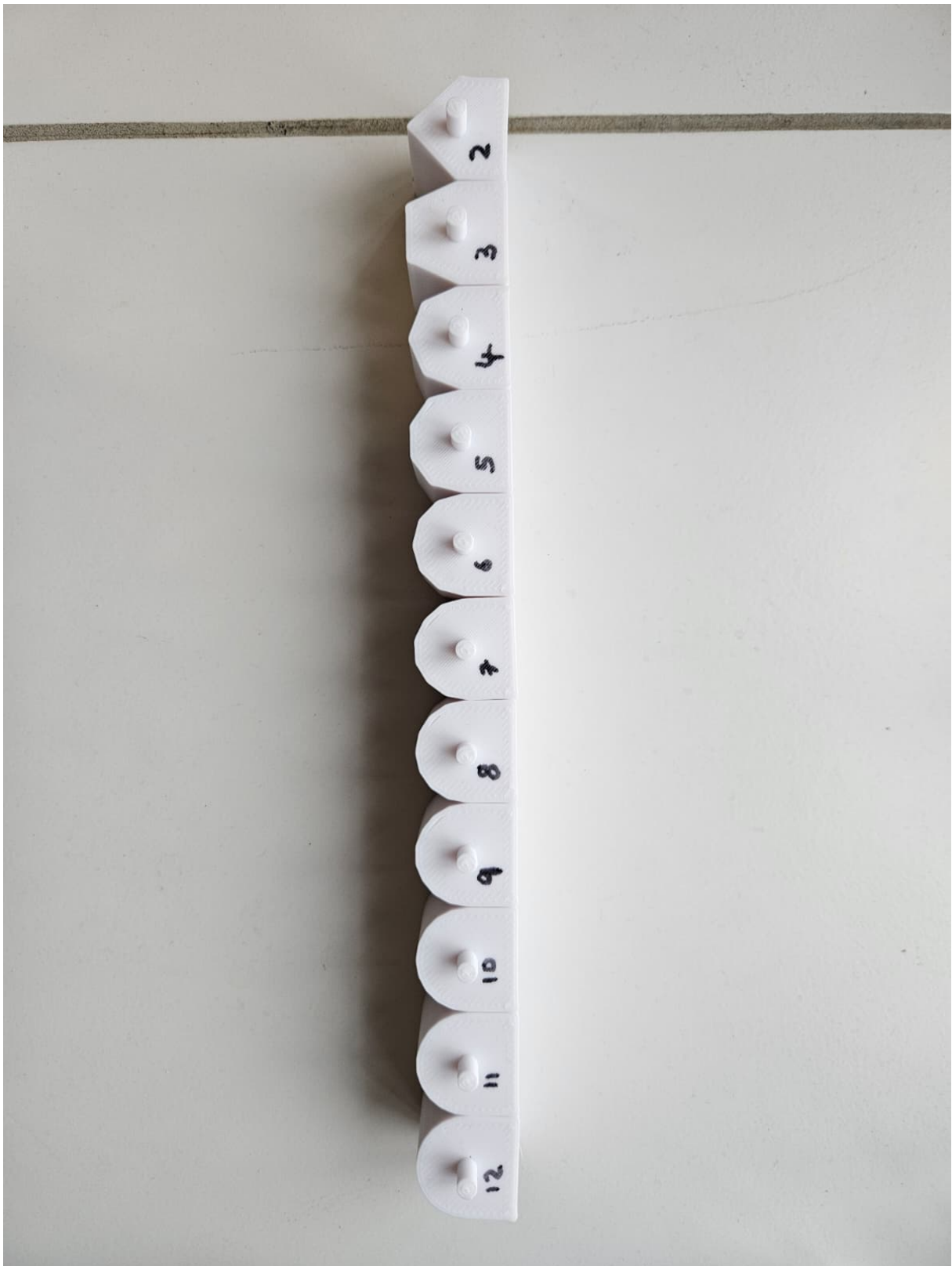


**Figure 12:** The 3D-printed bluff bodies of fixed height. The numbers correspond to the number of inlet-facing sides.

Inspired by the flow tank built by Harvard Natural Sciences Lecture Demonstrations (n.d.), the practical investigation was conducted in a self-built flow tank. A water pump created a flow over a horizontal plate by moving water from one side of separation wall (1) to the other. Separation wall (2), which did not reach the bottom of the tank, forced the flow of the horizontal wall towards the pump. The aquarium was filled with water so that it reached 0.01 m above the horizontal plate. The regulation valve was used to decrease the flow velocity while the sponge diffuser ensured a uniform distribution of flow — in an attempt to achieve laminar flow. Both a lamp and the addition of potassium permanganate crystals in front of the shape were used in order to better visualize the water flow. The thermal insulation foam ensured watertightness between the aquarium wall and the inside components.

The bluff bodies were 3D printed with an overall length  $\ell$  of 0.02 m — giving each shape a characteristic length  $L$  of 0.02 m — and a height of 0.04 m. Pre-tests showed that this overall length proved to be the optimal balance between the size of the bluff bodies and adequate identification of produced vortices, in an attempt to achieve a Reynolds number of 100. Reference marks on the horizontal plate ensured the shape was positioned consistently each trial. A Go-Pro recording in 120 FPS was mounted parallel to the horizontal plate, ensuring a continuous recording of the entire horizontal plate. The outer scaffolding provided support for the lamp, the GoPro and the water supply hose.

The flow velocity for the subsequent calculation of the Reynolds number was measured by introducing a float and measuring the time taken to travel the length of the horizontal plate via a digital stopwatch. This was repeated ten times and an average was taken.

## 5.4 Determining the vortex shedding frequency

The inverse relationship given by Equation (1) will be used to determine the vortex shedding frequency. By measuring the time interval between the formation of two consecutive vortices on one side of the bluff body, one can find the time period and therefore the frequency of vortex shedding. To obtain an accurate vortex shedding frequency, the determination of the time period was completed after periodic vortex shedding was achieved, omitting the initial startup phase in which the flow developed. A Fast Fourier Transform approach was not chosen due to the lack

of sufficient runtime during the trials on either investigation (Shi et al., 2025, pp. 10–11; Xu et al., 2025, p. 12).

### 5.4.1 Theoretical Investigation

The simulation was run five times for each bluff body. As all iterations yielded identical results, only the first run was considered, representing the average behavior for each bluff body. By graphing fluctuations of the lift coefficient (see Section 6.2.1), one can calculate the time period of vortex shedding by identifying the time taken between two consecutive peaks or troughs. This determination was done for each peak and trough using Python — see Appendix A — removing the first second to omit the startup phase. An average time period was then calculated and the vortex shedding frequency was found. ParaView was used to visualize the simulation.

### 5.4.2 Practical Investigation

The bluff bodies were placed into the flow tank at the position of the reference marks. Wearing gloves and goggles, minimal amounts of potassium permanganate were placed in front of them using a spatula — as shown in Figure 11. Once the flow fully developed, it was recorded for one minute each time. This minimized the number of water replacements — due to dissolving potassium permanganate turning the water purple — while ensuring that one could take multiple measurements of the time period. The water was reused for four shapes before the aquarium was emptied using a hand pump — disposing the solution in a properly assigned waste tank — and was refilled with fresh water.

The time period of vortex shedding was found via visual inspection of the GoPro footage and using a digital stop watch. It was repeated ten times for each bluff body. An average was subsequently calculated and the vortex shedding frequency was determined.

## 6 Results

### 6.1 Raw Data of the Theoretical Investigation

#### 6.1.1 Sample Table of Time vs. Lift Coefficient ( $C_L$ ) for Bluff Body $n = 2$

Time (s)	$C_L$
$1 \times 10^{-5}$	$2.0946206 \times 10^{-11}$
$2 \times 10^{-5}$	$-6.5426717 \times 10^{-12}$
$3 \times 10^{-5}$	$-7.3241302 \times 10^{-12}$
$4 \times 10^{-5}$	$-6.6677951 \times 10^{-12}$
$5 \times 10^{-5}$	$-5.1304516 \times 10^{-12}$
$6 \times 10^{-5}$	$-4.3635501 \times 10^{-12}$
$7 \times 10^{-5}$	$-3.6837751 \times 10^{-12}$
$8 \times 10^{-5}$	$-3.2635206 \times 10^{-12}$
$9 \times 10^{-5}$	$-2.8660898 \times 10^{-12}$
$1.0 \times 10^{-4}$	$-2.4321206 \times 10^{-12}$
$1.1 \times 10^{-4}$	$-2.1246574 \times 10^{-12}$
$1.2 \times 10^{-4}$	$-1.8807166 \times 10^{-12}$
$1.3 \times 10^{-4}$	$-1.6461582 \times 10^{-12}$
$1.4 \times 10^{-4}$	$-1.4100222 \times 10^{-12}$
$1.5 \times 10^{-4}$	$-1.1994923 \times 10^{-12}$
$1.6 \times 10^{-4}$	$-1.0306274 \times 10^{-12}$
$1.7 \times 10^{-4}$	$-8.6746456 \times 10^{-13}$
$1.8 \times 10^{-4}$	$-7.3730846 \times 10^{-13}$
$1.9 \times 10^{-4}$	$-6.2413158 \times 10^{-13}$
$2.0 \times 10^{-4}$	$-5.1195718 \times 10^{-13}$

**Table 3:** Example of the first 20 values of the table produced by the simulation. Time vs. Lift Coefficient ( $C_L$ ) for bluff body  $n = 2$ .

Only a representative sample is shown here for clarity. Complete datasets available on request.

## 6.2 Processed Data of the Theoretical Investigation

### 6.2.1 Representative (Average) Lift Coefficient ( $C_L$ ) Over Time for Each Bluff Body

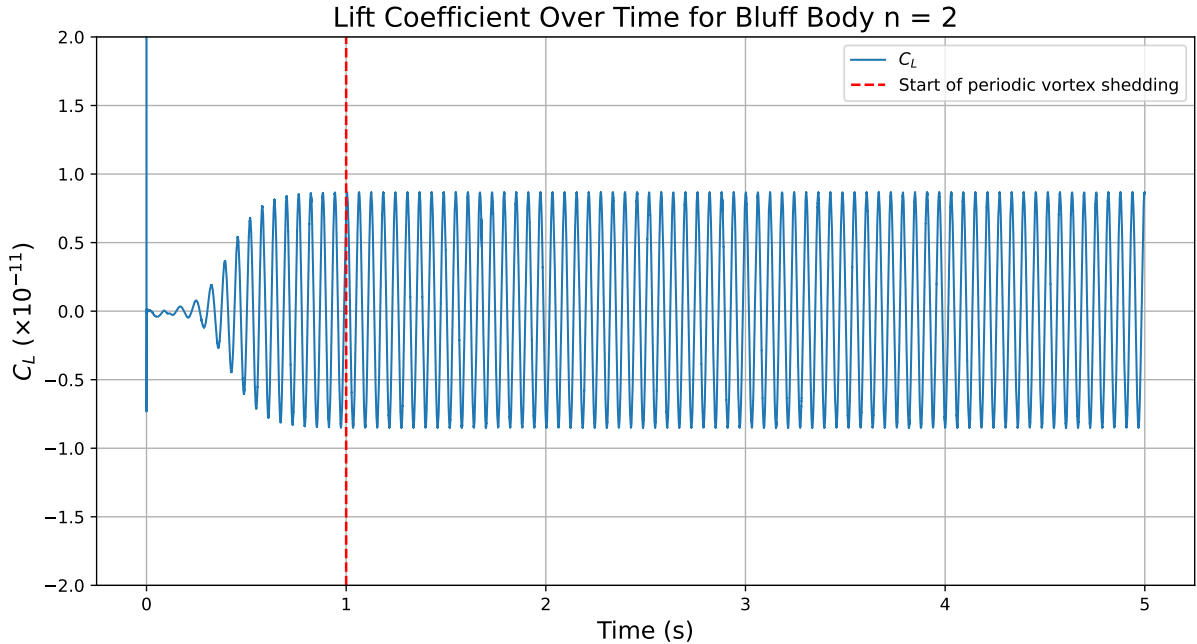


**Figure 13:** Average lift coefficient  $C_L$  over time for the bluff body  $n = 2$ , based on identical simulation results. The red dashed line indicates the start of periodic vortex shedding at  $t = 1$  s.

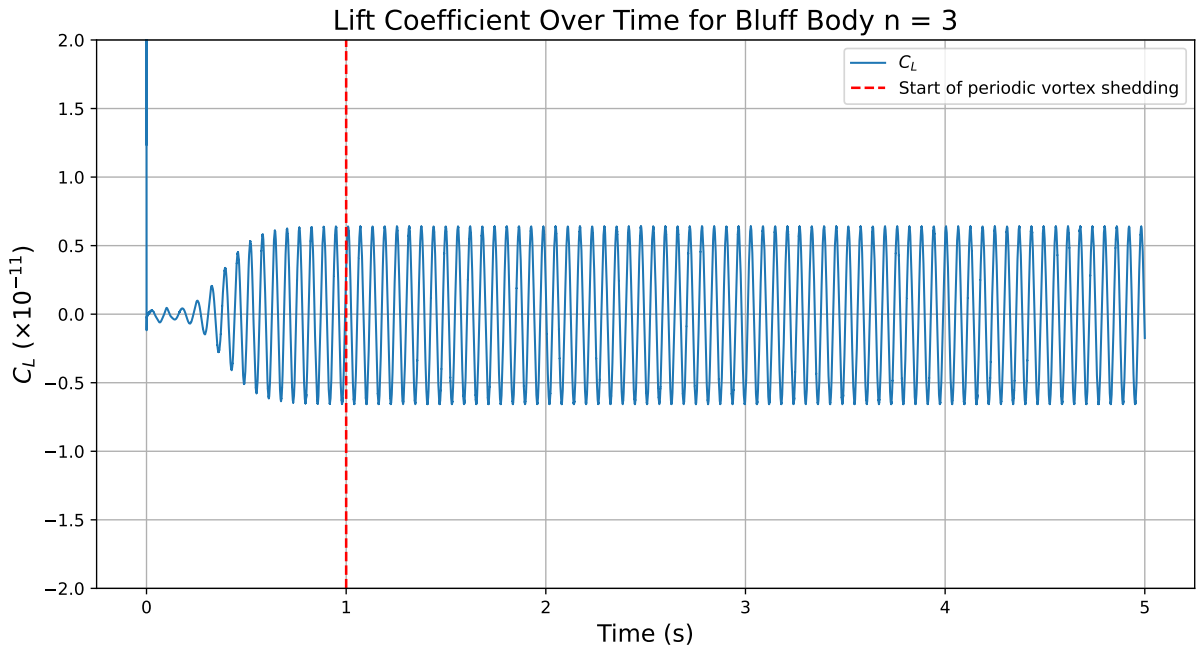


**Figure 14:** Average lift coefficient  $C_L$  over time for the bluff body  $n = 3$ , based on identical simulation results. The red dashed line indicates the start of periodic vortex shedding at  $t = 1$  s.

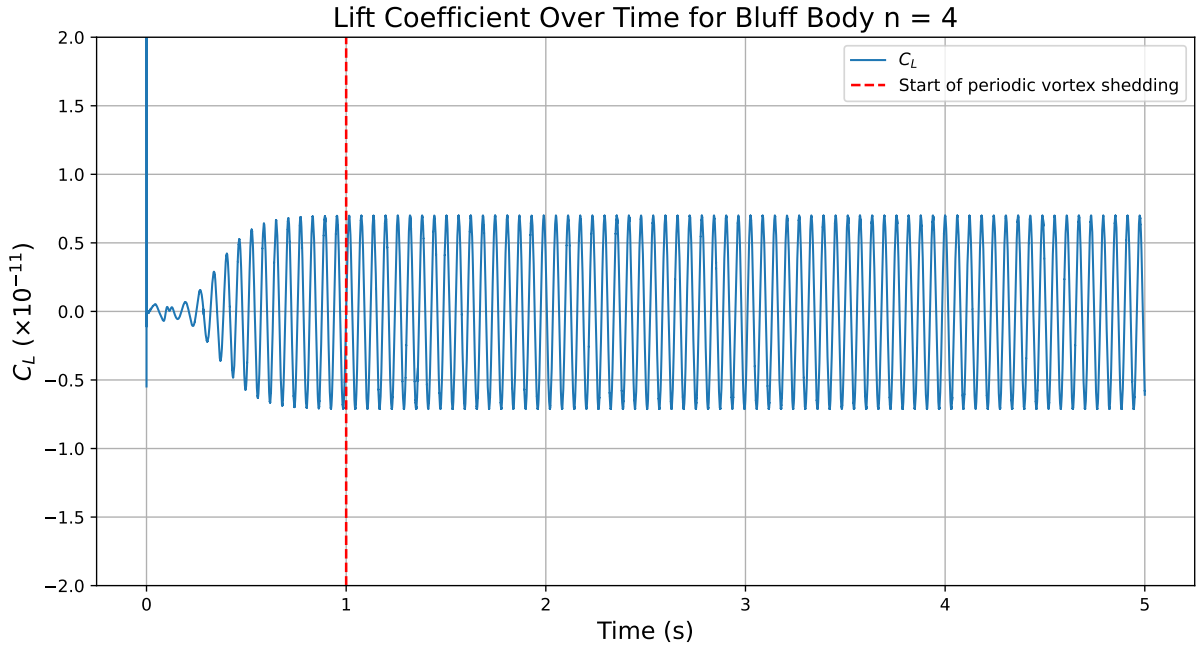


**Figure 15:** Average lift coefficient  $C_L$  over time for the bluff body  $n = 4$ , based on identical simulation results. The red dashed line indicates the start of periodic vortex shedding at  $t = 1$  s.

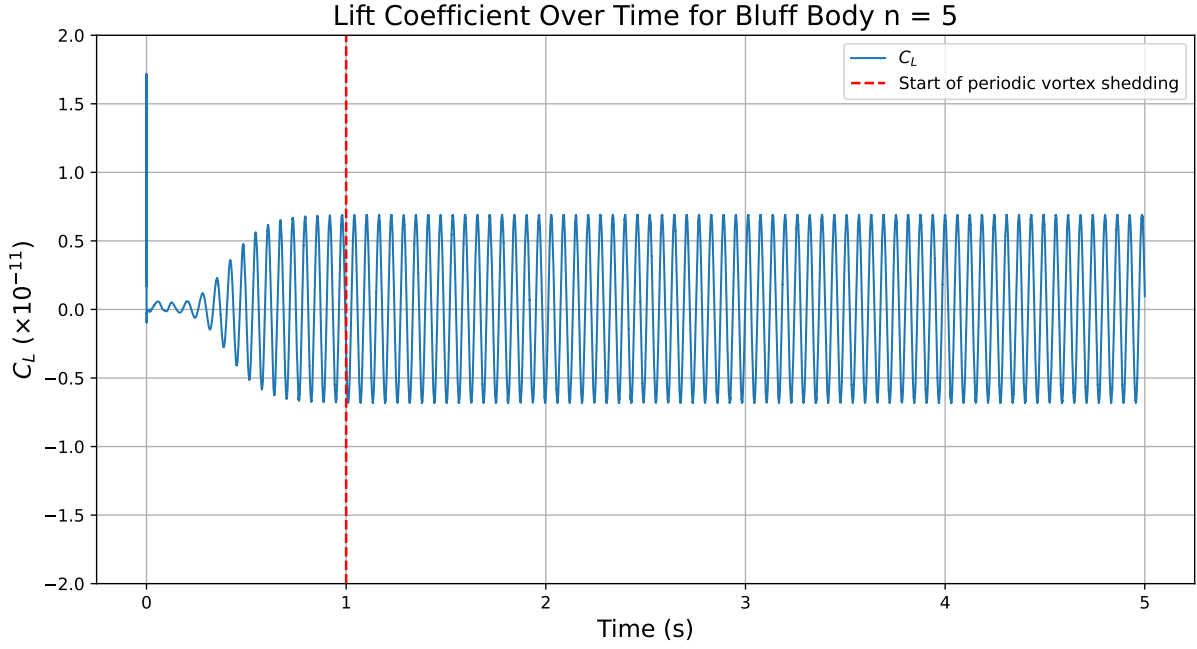


**Figure 16:** Average lift coefficient  $C_L$  over time for the bluff body  $n = 5$ , based on identical simulation results. The red dashed line indicates the start of periodic vortex shedding at  $t = 1$  s.

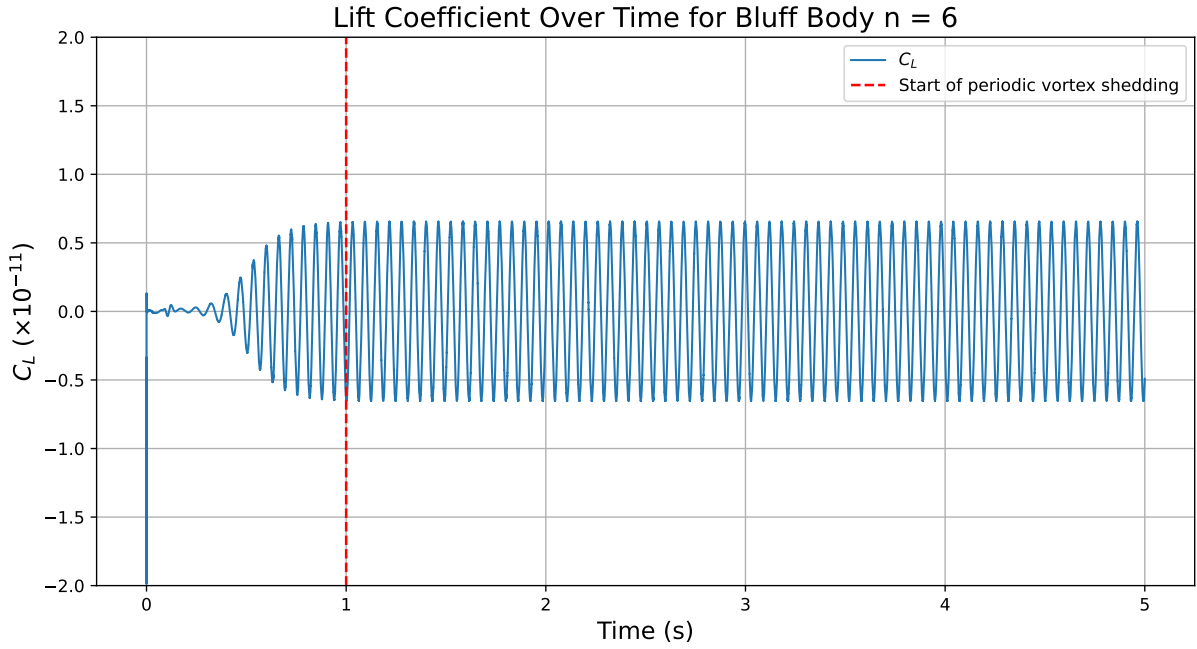


**Figure 17:** Average lift coefficient  $C_L$  over time for the bluff body  $n = 6$ , based on identical simulation results. The red dashed line indicates the start of periodic vortex shedding at  $t = 1$  s.

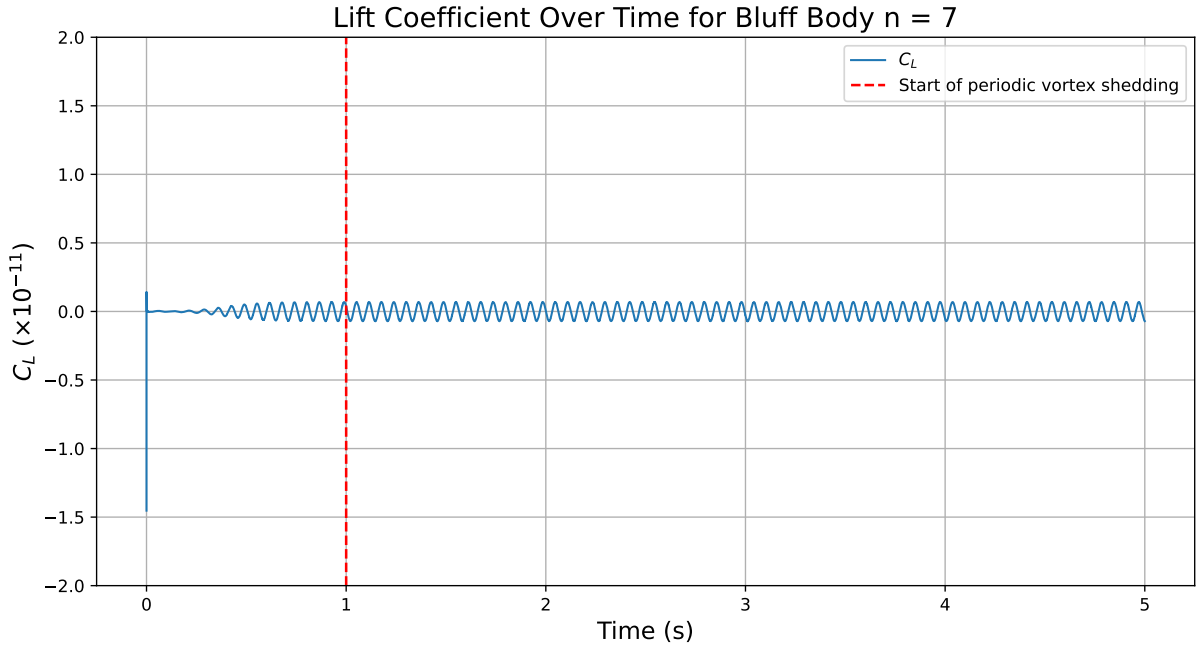


**Figure 18:** Average lift coefficient  $C_L$  over time for the bluff body  $n = 7$ , based on identical simulation results. The red dashed line indicates the start of periodic vortex shedding at  $t = 1$  s.

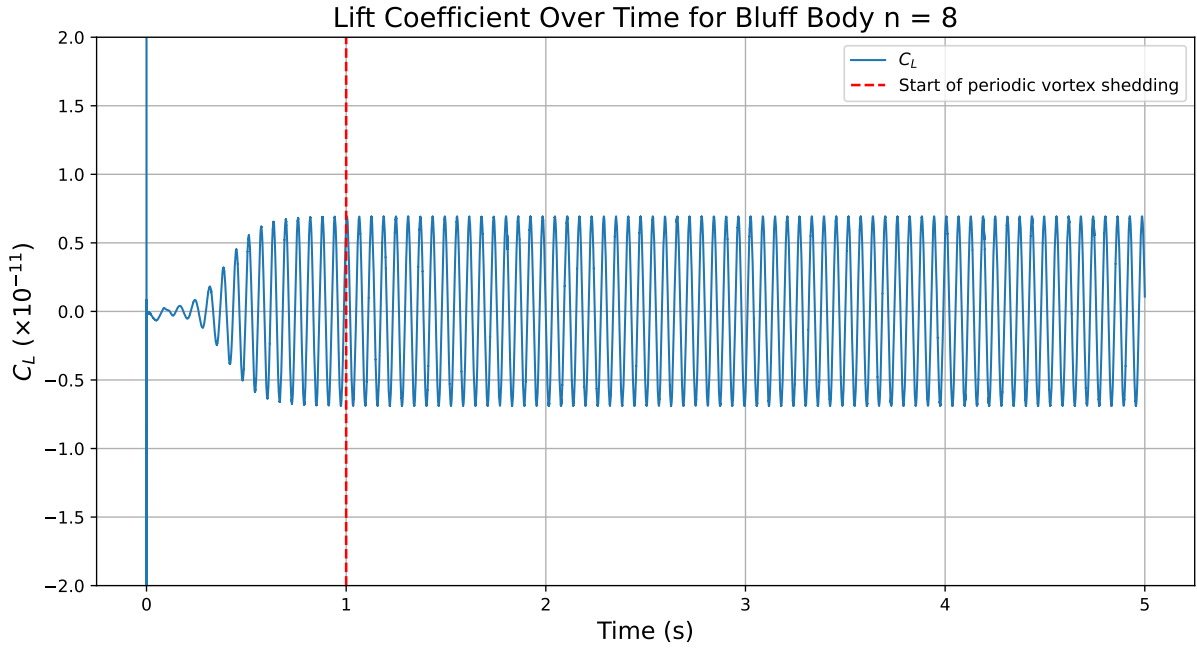


**Figure 19:** Average lift coefficient  $C_L$  over time for the bluff body  $n = 8$ , based on identical simulation results. The red dashed line indicates the start of periodic vortex shedding at  $t = 1$  s.

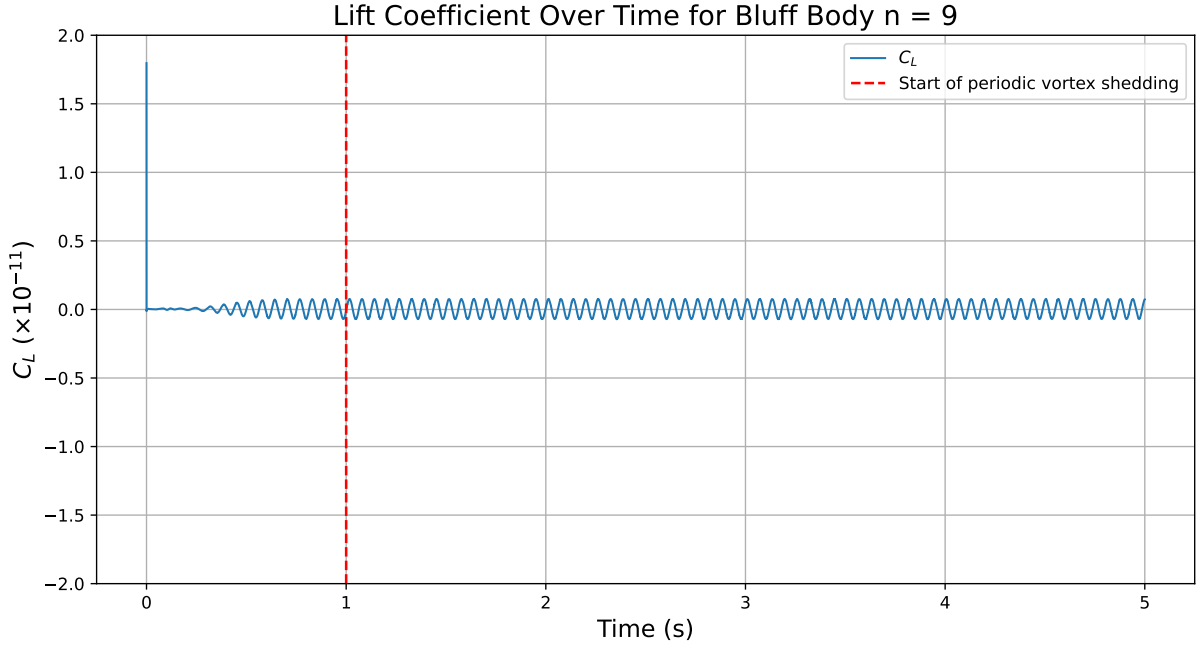


**Figure 20:** Average lift coefficient  $C_L$  over time for the bluff body  $n = 9$ , based on identical simulation results. The red dashed line indicates the start of periodic vortex shedding at  $t = 1$  s.

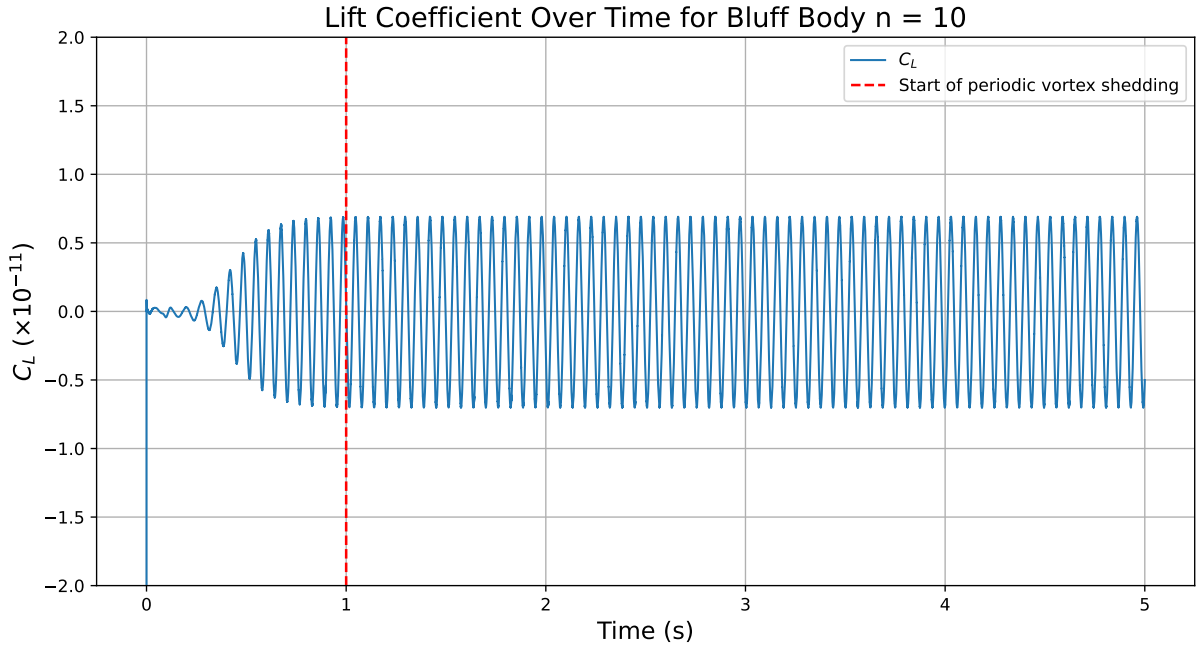


**Figure 21:** Average lift coefficient  $C_L$  over time for the bluff body  $n = 10$ , based on identical simulation results. The red dashed line indicates the start of periodic vortex shedding at  $t = 1$  s.

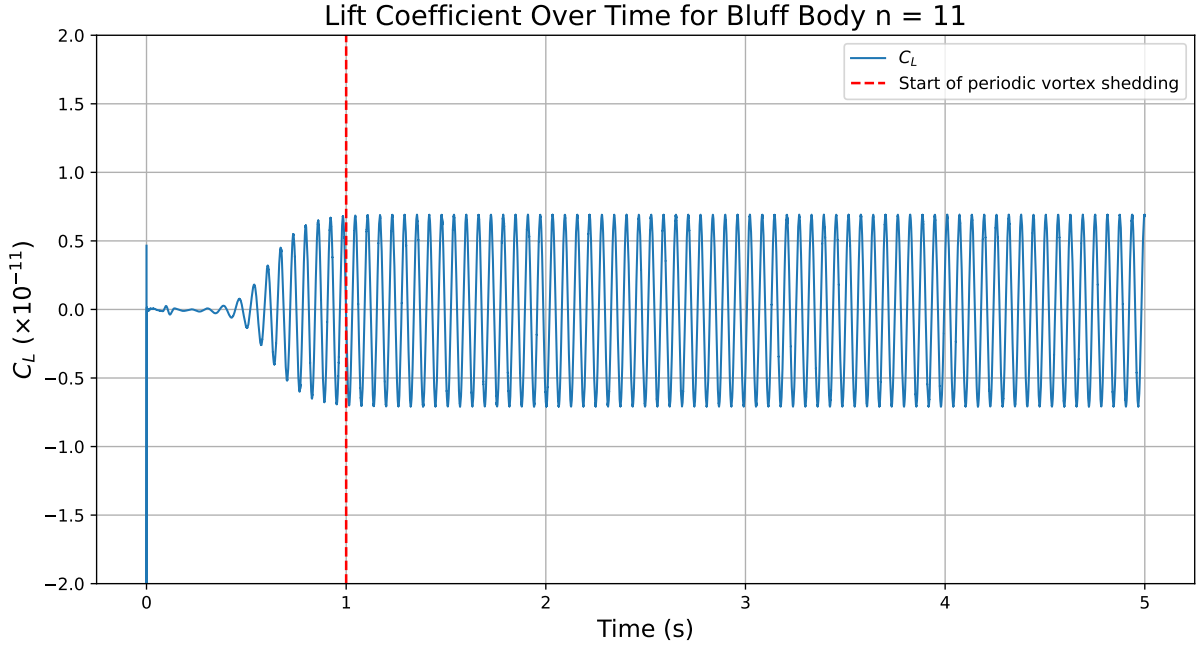


**Figure 22:** Average lift coefficient  $C_L$  over time for the bluff body  $n = 11$ , based on identical simulation results. The red dashed line indicates the start of periodic vortex shedding at  $t = 1$  s.

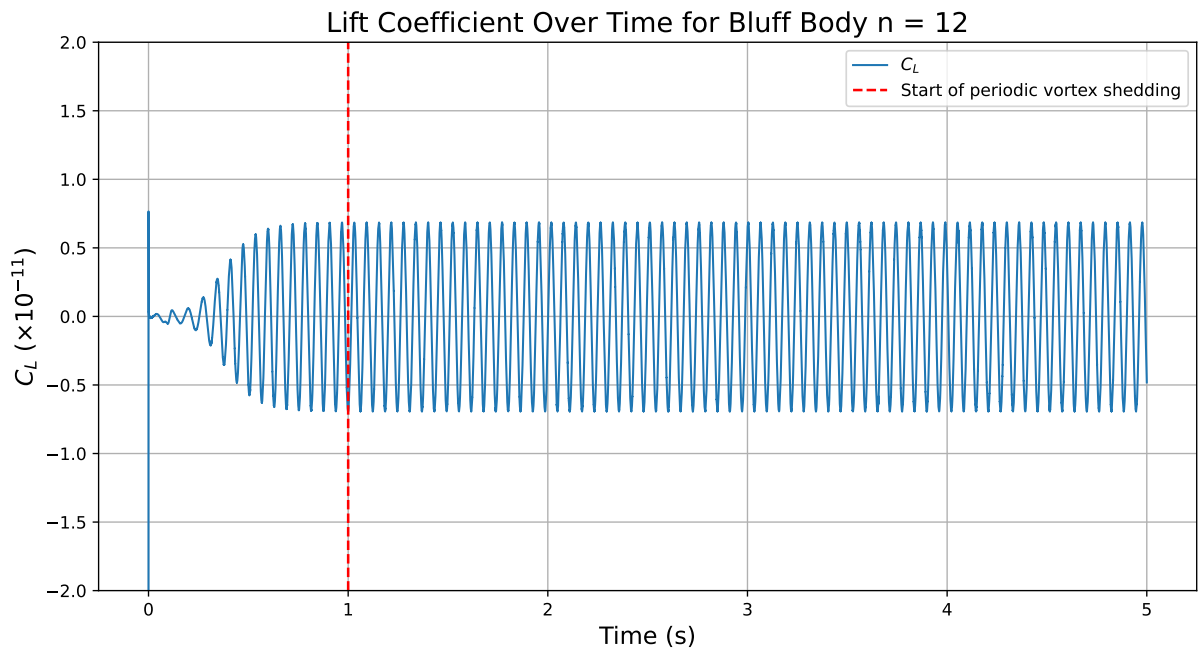


**Figure 23:** Average lift coefficient  $C_L$  over time for the bluff body  $n = 12$ , based on identical simulation results. The red dashed line indicates the start of periodic vortex shedding at  $t = 1$  s.

## 6.2.2 Sample Calculation of Vortex Shedding Frequency for Bluff Body $n = 2$ using Python

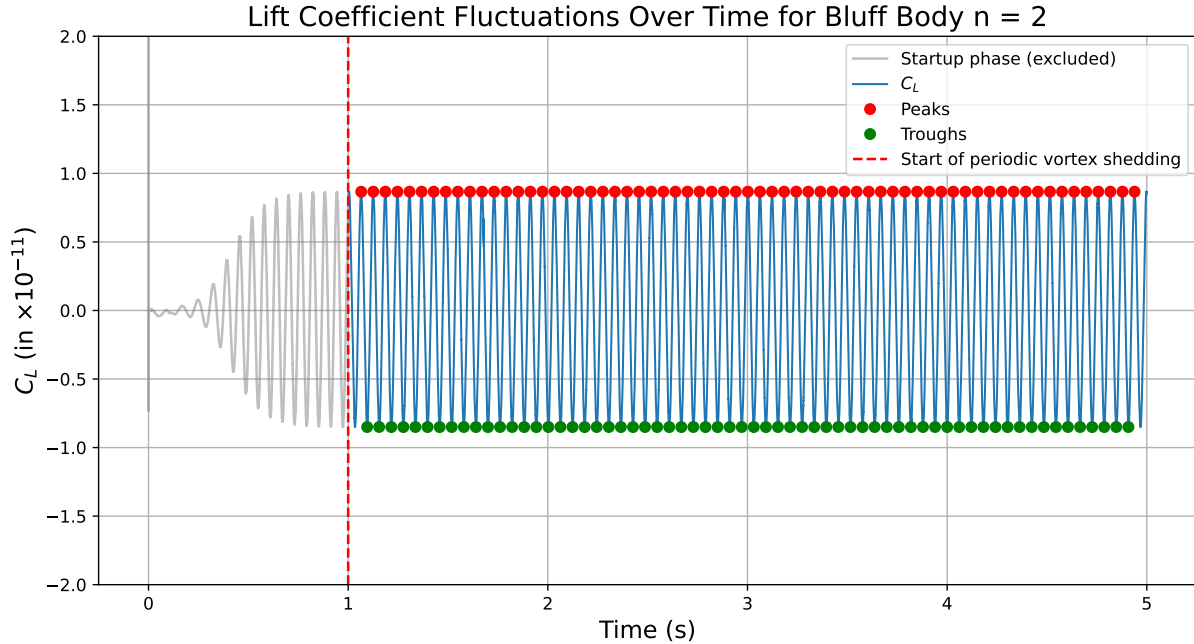


**Figure 24:** Sample visualization of the peaks and troughs identification on the Lift Coefficient  $C_L$  over time graph for bluff body  $n = 2$ . The initial startup phase, colored in gray, is excluded from the detection.

### Python Output

```
Number of peaks: 65
Number of troughs: 64

Average time period: 0.06052 s
```

Using the outputted average period  $T = 0.06052$  s, the vortex shedding frequency was calculated:

$$f = \frac{1}{T} = \frac{1}{0.06052} = 16.52346 \text{ Hz}$$

This represents the vortex shedding frequency of the bluff body with  $n = 2$  faces in laminar flow.

### 6.2.3 A Comparison of Vortex Shedding Frequency with Increasing $n$ from 2 – 12

Bluff Body $n$	Vortex Shedding Frequency (Hz)
2	16.52346
3	16.36393
4	16.41497
5	16.22323
6	16.28664
7	16.07976
8	16.32387
9	16.05910
10	16.09528
11	16.18909
12	16.21797

**Table 4:** Vortex shedding frequencies for bluff bodies with  $n$  streamwise faces.

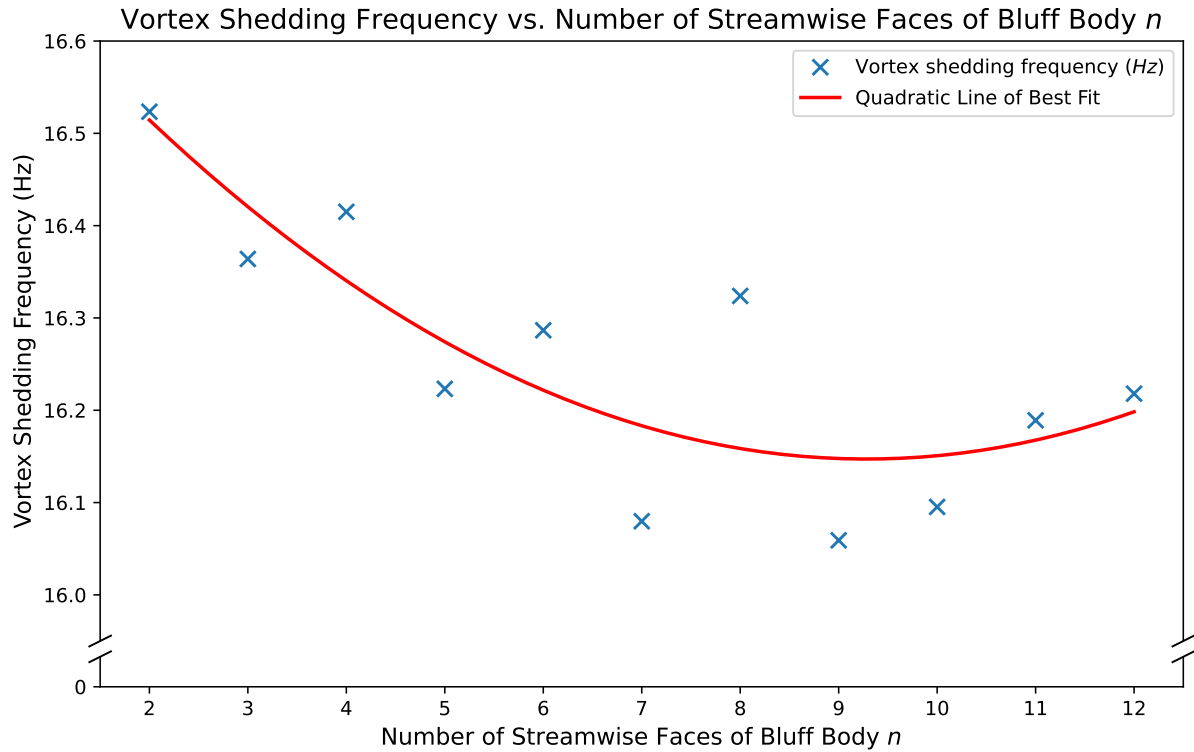


**Figure 25:** A comparison of vortex shedding frequency with increasing  $n$  from 2 – 12.

A quadratic line of best fit produced an  $R^2$  value of 0.6977, suggesting that the variation is reasonably well represented by a quadratic model. The graph portrays a negative correlation, indicating that bodies with an increased number of streamwise faces produce vortices at a lower frequency — attributable to an overall decrease in Strouhal number with increasing streamwise faces.

### 6.3 Results of Practical Investigation

The found average flow velocity was  $0.04 \text{ m s}^{-1}$ . Despite many attempts to achieve laminar flow, the flow remained turbulent, as demonstrated by the irregular wake patterns and a calculated Reynolds number of 800 — determined using Equation (2) where  $U = 0.04 \text{ m s}^{-1}$ ,  $\nu = 1 \times 10^6 \text{ m}^2 \text{ s}^{-1}$ , and  $L = 0.02 \text{ m}$ . Nevertheless, the practical experiment yielded qualitative value (See Appendix B).

## 7 Conclusion

The goal of this study was to investigate how the number of streamwise faces  $n$  of a bluff body influence the vortex shedding frequency in laminar flow. Bluff bodies ranging from  $n = 2 - 12$  were analyzed both theoretically and practically. However, only the theoretical investigation yielded quantitative results.

OpenFOAM simulations allowed for precise measurements of the fluctuations of the lift coefficient, and therefore an accurate determination of the vortex shedding frequency. Although the practical component of this investigation failed to achieve laminar flow conditions, it provided beneficial visual insight into the mechanism of vortex shedding, enhancing the investigation's tangibility while aiding conceptual understanding.

It was found that there is an overall decrease in vortex shedding frequency as the number of streamwise faces  $n$  of a bluff body increases — confirming the previously mentioned hypothesis. This trend is exemplified by bluff body  $n = 2$  which produced a vortex shedding frequency of 16.523 46 Hz, while the bluff body  $n = 12$  produced a vortex shedding frequency of 16.217 97 Hz. A direct comparison with literature is unfeasible as the effect of bluff body geometry on vortex shedding frequency has only been examined for a limited selection of shapes, leaving countless configurations, including those investigated in this study, previously unexplored (Przulj, 1998, p. 22).

The measured values from  $n = 2 - 7$  follow a fluctuating pattern with periodic increases and decreases. Bluff bodies with an even number of streamwise faces  $n$  tend to exhibit a greater vortex shedding frequency than their preceding odd-number counterparts, though conclusively claiming this would require further investigation.

Bluff body  $n = 8$  seems to be an anomaly with a vortex shedding frequency of 16.323 87 Hz. Although this is lower than the vortex shedding frequency of bluff body  $n = 2$ , therefore confirming the overall trend, its vortex shedding frequency is higher than that of bluff body  $n = 6$ .

Bluff body  $n = 9$  exhibits a significantly smaller decrease (only 0.020 66 Hz) in vortex shedding frequency to bluff body  $n = 7$ , possibly indicating a shift away from the previous overall downtrend. When considering bluff bodies  $n = 9 - 12$ , one identifies a positive correlation

between the vortex shedding frequency and the number of streamwise faces  $n$ , contrary to the previous downtrend. Further investigation would be required to confirm this claim.

The  $R^2$  value of 0.6977 indicates a moderate correlation between the number of streamwise faces  $n$  and the vortex shedding frequency. This rather low  $R^2$  value and the anomaly of bluff body  $n = 8$  may be attributed to numerical uncertainties of the simulation (Przulj, 1998). The anomalously low amplitudes of fluctuations of lift coefficient for bluff bodies  $n = 7$  and  $n = 9$  provide further evidence of possible numerical uncertainties.

## 8 Evaluation

### 8.1 Evaluation of the Theoretical Investigation

The simulation used for the theoretical investigation was based off of a tutorial case made by a professional, with minor changes made in order to adhere to the aim of this essay. As detailed in Section 5.4.1, the simulation was run five times for each bluff body, yielding identical results for each repetition and therefore providing a strong foundation for the results of this investigation. The simulation provided a method of study in which a two-dimensional flow could be investigated without the impact of boundary walls. Moreover, the simulated environment enabled strict control over the constant variables, thereby minimizing the influence of confounding factors, ensuring the alteration of vortex shedding frequency could be solely attributed to the change in the number of streamwise faces.

The measurement of the lift coefficient  $C_L$  was done within the simulation, eliminating the uncertainties introduced by external measurement equipment. Furthermore, the determination of the time period was completed for all peaks and troughs, with an average providing the final time period, therefore reducing the impact of anomalies on the results.

Nevertheless, as mentioned in Section 7, numerical uncertainties introduced by numerous factors such as the mesh resolution may remain a reason for error, especially due to the unfeasible nature of quantifying these potentially mutually canceling factors (Przulj, 1998). Computational limitations restricted both the unit size of the mesh of the domain and the time step value ( $\Delta t$ ), therefore possibly introducing discrepancies between the modeled and actual fluid behavior.

This was partially solved by the inclusion of a BOI, decreasing the unit size of the mesh around the bluff body and in the wake region. Coupled with a decreased unit size at the edge of the bluff body, the interaction of the bluff body with the flow was simulated more accurately.

## 8.2 Evaluation of the Practical Investigation

The inability to achieve laminar flow rendered the practical investigation nonviable for quantitative comparison with simulated data. It would have been necessary to decrease the characteristic length of the bluff bodies, the flow velocity or a combination of both. However, as discussed earlier in Section 5.3, decreasing the size of the bluff bodies would have resulted in smaller vortices, too small to identify by eyesight. In addition, the lack of a less powerful water pump rendered a further decrease in flow velocity — beyond that provided by the regulation valve — unachievable. Furthermore, various weaknesses including the inherent difficulty in identifying the exact point when a vortex is shed through visual inspection would render any data inaccurate.

## References

- Alammar, A. (n.d.). *Wake of bodies (chapter 1)*. Retrieved July 14, 2025, from [https://www.researchgate.net/profile/Ahmed-Alammar/.../wake+of+bodies+6248\\_chap01.pdf](https://www.researchgate.net/profile/Ahmed-Alammar/.../wake+of+bodies+6248_chap01.pdf)
- Allum, J., & Morris, P. (2023). *Physics* (3rd ed.). Hodder Education.
- Ansys Learning. (2023, February 10). *Best practices for mesh generation — lesson 2*. Retrieved June 22, 2025, from <https://www.youtube.com/watch?v=nwrBYdHi64w>
- Ansys workbench | simulation integration platform*. (n.d.). Retrieved June 22, 2025, from <https://www.ansys.com/products/ansys-workbench>
- Buresti, G. (1998). Vortex shedding from bluff bodies. *Journal of Wind Engineering and Industrial Aerodynamics*, 74-76, 163–172. [https://doi.org/10.1016/S0167-6105\(98\)00015-5](https://doi.org/10.1016/S0167-6105(98)00015-5)
- Caminha, G. (2017, August 29). *CFL condition: How to choose your timestep size* [SimScale]. Retrieved July 13, 2025, from <https://www.simscale.com/blog/cfl-condition/>
- Choi, C.-K., & Kwon, D. K. (2000). Determination of the strouhal number based on the aerodynamic behavior of rectangular cylinders. *Wind and Structures: An International Journal*, 3(3), 209–220. <https://doi.org/10.12989/was.2000.3.3.209>
- Codeynamics. (2024, January 21). *Prism drag and lift calculation and plotting | cd cl | OpenFOAM CFD | simpleFoam*. Retrieved July 13, 2025, from <https://www.youtube.com/watch?v=hOvGF1DUn8A>
- comflics. (2014, August 27). *OpenFOAM tutorial #4 - laminar vortex shedding*. Retrieved June 22, 2025, from <https://www.youtube.com/watch?v=yIzQXiEdYYo>
- Embry-Riddle Aeronautical University. (n.d.). *Introduction to boundary layers*. EaglePubs Open Educational Resources. Retrieved May 22, 2025, from <https://eaglepubs.erau.edu/introductiontoaerospaceflightvehicles/chapter/introduction-to-boundary-layers/>
- Fitzpatrick, R. (2016, March). *Reynolds number*. University of Texas at Austin. Retrieved May 20, 2025, from <https://farside.ph.utexas.edu/teaching/336L/Fluidhtml/node116.html>
- Fluid Mechanics 101. (2021, June 24). *[CFD] inflation layers / prism layers in CFD*. Retrieved June 22, 2025, from <https://www.youtube.com/watch?v=1gSHN99I7L4>

*FreeCAD: Ihr parametrischer 3D-Modellierer.* (n.d.). Retrieved July 22, 2025, from <https://www.freecad.org/index.php?lang=de>

Gonçalves, H. C., & Del Rio Vieira, E. (1999). Strouhal number determination for several regular polygon cylinders for reynolds number up to 600. *Proceedings of the 15th Brazilian Congress of Mechanical Engineering (COBEM 1999)*. Retrieved July 22, 2025, from <https://www.abcm.org.br/anais/cobem/1999/pdf/AACFFE.pdf>

Govardhan, R., & Ramesh, O. (2005). A stroll down kármán street. *Resonance*, 10, 25–37. <https://doi.org/10.1007/BF02866744>

Green, S. I. (Ed.). (1995). *Fluid vortices* (Vol. 30). Kluwer Academic Publishers. <https://doi.org/10.1007/978-94-011-0249-0>

Harvard Natural Sciences Lecture Demonstrations. (n.d.). *Vortex shedding in water | harvard natural sciences lecture demonstrations*. Retrieved June 23, 2025, from <https://sciedemonstrations.fas.harvard.edu/presentations/vortex-shedding>

Holton, J. R. (2003). Vorticity. In J. R. Holton (Ed.), *Encyclopedia of atmospheric sciences* (pp. 2500–2504). Academic Press. <https://doi.org/10.1016/B0-12-227090-8/00449-8>

Ib physics guide 2025. (2023). *International Baccalaureate Organization*. Retrieved February 27, 2025, from <https://peda.net/kuopio/lukiot/lyseonlukio/ib/syllabukset/group-4-sciences/physics-2025.pdf:file/download/c56a8c8592e847bbb555540b087b0990d1ade5b0/Physics%2C%202025.pdf>

Ibrahim, N. (2022). Peminggiran sosial dalam kalangan warga emas: Intervensi ke arah penuaan sihat. Retrieved July 22, 2025, from [https://core.ac.uk/outputs/42956006/?utm\\_source=pdf&utm\\_medium=banner&utm\\_campaign=pdf-decoration-v1](https://core.ac.uk/outputs/42956006/?utm_source=pdf&utm_medium=banner&utm_campaign=pdf-decoration-v1)

Ilieva, G. (2017). On turbulence and its effects on aerodynamics of flow through turbine stages. In *Turbomachinery*. InTech. <https://doi.org/10.5772/intechopen.68205>

Jayaraj P, H. (2024). *Lecture: Introduction to vortex shedding simulation using openfoam*. Udemy. Retrieved March 12, 2025, from <https://www.udemy.com/course/openfoam - for - absolute-beginners/learn/lecture/44356412>

Jeff Defoe. (2020, May 26). *Bluff body aerodynamics, lecture 2 part 5*. Retrieved June 22, 2025, from <https://www.youtube.com/watch?v=9g62QkNFtI>

- Jurado, J. Á., Sánchez, R., Hernández, S., Nieto, F., & Kusano, I. (2012). A review of cases of vortex shedding excitation in bridges: Sectional models testing. *Proceedings of the Seventh International Colloquium on Bluff Body Aerodynamics and Applications (BAA7)*. Retrieved May 4, 2025, from <https://iawe.org/Proceedings/BAA7/J.Jurado.pdf>
- Learn Engineering. (2022, August). *What is boundary layer in fluid mechanics*. Retrieved April 16, 2025, from <https://www.youtube.com/watch?v=ahohd8ceGR4>
- Lnicez schmutzwasser-tauchpumpe(75 w, ø19 mm,3.000l/h)*. (n.d.). Retrieved July 22, 2025, from [https://www.amazon.de/dp/B0987LCYMK?ref=ppx\\_yo2ov\\_dt\\_b\\_fed\\_asin\\_title&th=1](https://www.amazon.de/dp/B0987LCYMK?ref=ppx_yo2ov_dt_b_fed_asin_title&th=1)
- Mohn, E. (2024). *Non-newtonian fluid*. EBSCO Information Services. Retrieved April 30, 2025, from <https://www.ebsco.com/research-starters/science/non-newtonian-fluid>
- NASA Glenn Research Center. (2021). *Reynolds number*. NASA. Retrieved May 13, 2025, from <https://www.grc.nasa.gov/www/k-12/airplane/reynolds.html>
- National Research Council. (1997). *Twenty-first symposium on naval hydrodynamics*. National Academies Press. Retrieved June 22, 2025, from <https://doi.org/10.17226/5870>
- Nitsche, M. (2006). Vortex dynamics. In J.-P. Françoise, G. L. Naber, & S. T. Tsou (Eds.), *Encyclopedia of mathematical physics* (pp. 390–399). Academic Press. <https://doi.org/10.1016/B0-12-512666-2/00254-6>
- OpenAI. (2025). Chatgpt (gpt-4o) [Code suggestions generated by OpenAI's ChatGPT (GPT-4o). Prompt mentioned in-text. Accessed via OpenAI ChatGPT on 26 July 2025.]. Retrieved July 26, 2025, from <https://chat.openai.com/>
- OpenFOAM*. (2024, December 24). Retrieved June 22, 2025, from <https://www.openfoam.com/>
- Oran, E. S., & Boris, J. P. (2002). Fluid dynamics. In R. A. Meyers (Ed.), *Encyclopedia of physical science and technology* (3rd ed., pp. 31–43). Academic Press. <https://doi.org/10.1016/B0-12-227410-5/00248-9>
- Original Prusa MINI+ Halbmontiert | Original Prusa 3D-Drucker direkt von Josef Prusa [Prusa3D by Josef Prusa]*. (n.d.). Retrieved July 22, 2025, from <https://www.prusa3d.com/de/produkt/original-prusa-mini-halbmontiert-4/>

- ParaView - open-source, multi-platform data analysis and visualization application.* (n.d.). Retrieved July 21, 2025, from <https://www.paraview.org/>
- pimpleFoam - OpenFOAM solver - SimFlow CFD software.* (n.d.). Retrieved July 27, 2025, from <https://help.sim-flow.com/solvers/pimple-foam>
- PrusaSlicer | Original Prusa 3D-Drucker direkt von Josef Prusa [Prusa3D by Josef Prusa].* (n.d.). Retrieved July 22, 2025, from [https://www.prusa3d.com/de/page/prusaslicer\\_424/](https://www.prusa3d.com/de/page/prusaslicer_424/)
- Przulj, V. (1998, July). *Computational modelling of vortex shedding flows*, City University London. Retrieved July 25, 2025, from <https://openaccess.city.ac.uk/id/eprint/7565/>
- The relationship between reynolds number and kinematic viscosity.* (n.d.). Retrieved July 14, 2025, from <https://resources.system-analysis.cadence.com/blog/msa2022-the-relationship-between-reynolds-number-and-kinematic-viscosity>
- Rocchi, D., & Zasso, A. (2002). Vortex shedding from a circular cylinder in a smooth and wired configuration: Comparison between 3d les simulation and experimental analysis. *Journal of Wind Engineering and Industrial Aerodynamics*, 90(4–5), 475–489. [https://doi.org/10.1016/S0167-6105\(01\)00203-3](https://doi.org/10.1016/S0167-6105(01)00203-3)
- Saldana, M., Gallegos, S., Gálvez, E., Castillo, J., Salinas-Rodríguez, E., Cerecedo-Sáenz, E., Hernández-Ávila, J., Navarra, A., & Toro, N. (2024). The reynolds number: A journey from its origin to modern applications. *Fluids*, 9(12), 299. <https://doi.org/10.3390/fluids9120299>
- Shen, H.-M., Fu, X., Chen, J.-D., & Ye, P. (2010). Development of a vortex flowmeter with good performance at low-flowrate. *Proceedings of the 15th International Flow Measurement Conference (FLOMEKO)*, 1–6. Retrieved April 2, 2025, from <https://www.imeko.org/publications/tc9-2010/IMEKO-TC9-2010-017.pdf>
- Shi, F., Ou, C., Xin, J., Li, W., Jin, Q., Tian, Y., & Zhang, W. (2025). Numerical study on hydrodynamic performance and vortex dynamics of multiple cylinders under forced vibration at low reynolds number. *Journal of Marine Science and Engineering*, 13(2), 214. <https://doi.org/10.3390/jmse13020214>

- Song, D., Kim, W., Kwon, O.-K., & Choi, H. (2022). *Vertical and torsional vibrations before the collapse of the tacoma narrows bridge in 1940*. <https://doi.org/10.1017/jfm.2022.748>
- TutorialsPoint. (2018, January 23). *Boundary layer theory - introduction*. Retrieved June 22, 2025, from <https://www.youtube.com/watch?v=54zf68IoPWU>
- Versteeg, H. K., & Malalasekera, W. (2007). *An introduction to computational fluid dynamics: The finite volume method* (2nd ed.). Pearson Education.
- Water - dynamic and kinematic viscosity at various temperatures and pressures*. (n.d.). Retrieved July 13, 2025, from [https://www.engineeringtoolbox.com/water-dynamic-kinematic-viscosity-d\\_596.html](https://www.engineeringtoolbox.com/water-dynamic-kinematic-viscosity-d_596.html)
- Welcome to python.org* [Python.org]. (2025, July 16). Retrieved July 21, 2025, from <https://www.python.org/>
- Windows subsystem for linux (WSL)* [Ubuntu]. (n.d.). Retrieved July 21, 2025, from <https://ubuntu.com/desktop/wsl>
- Xu, G., Yu, W., Sciacchitano, A., & Simao Ferreira, C. (2025). An experimental study of the unsteady aerodynamics of a static DU91-w2-150 airfoil at large angles of attack. *Wind Energy*, 28(3), e2974. <https://doi.org/10.1002/we.2974>

## A Python Code

```
1 import numpy as np
2 import matplotlib.pyplot as plt
3 from scipy.signal import find_peaks
4 import os
5
6 # Parameters
7 number_of_faces_of_bluff_body = 9
8 cutoff = 1.0 # Seconds
9 prominence_threshold = 0.3
10
11 # Load C_L data
12 filename = rf"..."
13 time, cL = [], []
14
15 os.chdir(r"...")
16
17 with open(filename, "r") as f:
18     for line in f:
19         if line.strip().startswith("#") or not line.strip():
20             continue
21         parts = line.strip().split()
22         if len(parts) >= 5:
23             time.append(float(parts[0]))
24             cL.append(float(parts[4]))
25
26 time = np.array(time)
27 cL = np.array(cL)
28
29 # Remove startup phase
```

```

30 mask = time > cutoff
31 time = time[mask]
32 c1 = c1[mask]
33
34 # Normalize C_L
35 c1_norm = c1 - np.mean(c1)
36 c1_norm = c1_norm / np.max(np.abs(c1_norm))
37
38 # Detect peaks
39 peak_indices, _ = find_peaks(c1_norm, prominence=prominence_threshold)
40
41 # Find troughs between each pair of peaks
42 trough_indices = []
43 for i in range(len(peak_indices) - 1):
44     left = peak_indices[i]
45     right = peak_indices[i + 1]
46     if right > left + 1:
47         trough_region = c1_norm[left:right+1]
48         trough_local_index = np.argmin(trough_region)
49         trough_global_index = left + trough_local_index
50         trough_indices.append(trough_global_index)
51
52 trough_indices = np.array(trough_indices)
53
54 # Calculate average period from peaks and troughs separately
55 peak_times = time[peak_indices]
56 trough_times = time[trough_indices]
57
58 # Only compute periods if enough points exist
59 if len(peak_times) >= 2:
60     peak_periods = np.diff(peak_times)

```

```

61 else:
62     peak_periods = np.array([])
63
64 if len(through_times) >= 2:
65     through_periods = np.diff(through_times)
66 else:
67     through_periods = np.array([])
68
69 # Combine both for average period
70 all_periods = np.concatenate([peak_periods, through_periods])
71 if len(all_periods) >= 1:
72     avg_full_period = np.mean(all_periods)
73 else:
74     avg_full_period = np.nan
75
76 # Print results
77 print(f"Number of peaks: {len(peak_indices)}")
78 print(f"Number of troughs: {len(through_indices)}")
79 print(f"\nAverage full period: {avg_full_period:.5f} s")

```

**Listing 1:** Calculating time period by identifying peaks and troughs of lift coefficient  $C_L$  graph. The exact file paths were excluded due to privacy reasons. Code generated on the 26<sup>th</sup> of July 2025 by OpenAI (2025) using the prompt “*Write Python code to calculate the time period by identifying peaks and troughs of the lift coefficient  $C_L$  graph. The code should read data from a text file containing multiple columns, where the first column represents time and the fifth column represents the lift coefficient  $C_L$ . It should find all peaks and troughs, calculate the time period for each peak-to-subsequent-peak and trough-to-subsequent-trough pair, compute the average time period for the peaks and troughs separately, and then take the average of those two values to obtain the overall mean time period.*”. It was subsequently edited with minor adjustments to reflect the author’s intent and to ensure full functionality on the local computer on which the code was executed.

## B Snapshots of Practical Investigation

### Snapshots of the Practical Run of Bluff Body $n = 2$



(a) Snapshot of bluff body  $n = 2$  at time 0 s.



(b) Snapshot of bluff body  $n = 2$  at time 1 s.



(c) Snapshot of bluff body  $n = 2$  at time 2 s.



(d) Snapshot of bluff body  $n = 2$  at time 3 s.



(e) Snapshot of bluff body  $n = 2$  at time 4 s.



(f) Snapshot of bluff body  $n = 2$  at time 5 s.

## Snapshots of the Practical Run of Bluff Body $n = 3$



(a) Snapshot of bluff body  $n = 3$  at time 0 s.



(b) Snapshot of bluff body  $n = 3$  at time 1 s.



(c) Snapshot of bluff body  $n = 3$  at time 2 s.



(d) Snapshot of bluff body  $n = 3$  at time 3 s.



(e) Snapshot of bluff body  $n = 3$  at time 4 s.



(f) Snapshot of bluff body  $n = 3$  at time 5 s.

## Snapshots of the Practical Run of Bluff Body $n = 4$



(a) Snapshot of bluff body  $n = 4$  at time 0 s.



(b) Snapshot of bluff body  $n = 4$  at time 1 s.



(c) Snapshot of bluff body  $n = 4$  at time 2 s.



(d) Snapshot of bluff body  $n = 4$  at time 3 s.



(e) Snapshot of bluff body  $n = 4$  at time 4 s.



(f) Snapshot of bluff body  $n = 4$  at time 5 s.

## Snapshots of the Practical Run of Bluff Body $n = 5$



(a) Snapshot of bluff body  $n = 5$  at time 0 s.



(b) Snapshot of bluff body  $n = 5$  at time 1 s.



(c) Snapshot of bluff body  $n = 5$  at time 2 s.



(d) Snapshot of bluff body  $n = 5$  at time 3 s.



(e) Snapshot of bluff body  $n = 5$  at time 4 s.



(f) Snapshot of bluff body  $n = 5$  at time 5 s.

## Snapshots of the Practical Run of Bluff Body $n = 6$



(a) Snapshot of bluff body  $n = 6$  at time 0 s.



(b) Snapshot of bluff body  $n = 6$  at time 1 s.



(c) Snapshot of bluff body  $n = 6$  at time 2 s.



(d) Snapshot of bluff body  $n = 6$  at time 3 s.



(e) Snapshot of bluff body  $n = 6$  at time 4 s.



(f) Snapshot of bluff body  $n = 6$  at time 5 s.

## Snapshots of the Practical Run of Bluff Body $n = 7$



(a) Snapshot of bluff body  $n = 7$  at time 0 s.



(b) Snapshot of bluff body  $n = 7$  at time 1 s.



(c) Snapshot of bluff body  $n = 7$  at time 2 s.



(d) Snapshot of bluff body  $n = 7$  at time 3 s.



(e) Snapshot of bluff body  $n = 7$  at time 4 s.



(f) Snapshot of bluff body  $n = 7$  at time 5 s.

## Snapshots of the Practical Run of Bluff Body $n = 8$



(a) Snapshot of bluff body  $n = 8$  at time 0 s.



(b) Snapshot of bluff body  $n = 8$  at time 1 s.



(c) Snapshot of bluff body  $n = 8$  at time 2 s.



(d) Snapshot of bluff body  $n = 8$  at time 3 s.



(e) Snapshot of bluff body  $n = 8$  at time 4 s.



(f) Snapshot of bluff body  $n = 8$  at time 5 s.

## Snapshots of the Practical Run of Bluff Body $n = 9$



(a) Snapshot of bluff body  $n = 9$  at time 0 s.



(b) Snapshot of bluff body  $n = 9$  at time 1 s.



(c) Snapshot of bluff body  $n = 9$  at time 2 s.



(d) Snapshot of bluff body  $n = 9$  at time 3 s.



(e) Snapshot of bluff body  $n = 9$  at time 4 s.



(f) Snapshot of bluff body  $n = 9$  at time 5 s.

## Snapshots of the Practical Run of Bluff Body $n = 10$



(a) Snapshot of bluff body  $n = 10$  at time 0 s.



(b) Snapshot of bluff body  $n = 10$  at time 1 s.



(c) Snapshot of bluff body  $n = 10$  at time 2 s.



(d) Snapshot of bluff body  $n = 10$  at time 3 s.



(e) Snapshot of bluff body  $n = 10$  at time 4 s.



(f) Snapshot of bluff body  $n = 10$  at time 5 s.

## Snapshots of the Practical Run of Bluff Body $n = 11$



(a) Snapshot of bluff body  $n = 11$  at time 0 s.



(b) Snapshot of bluff body  $n = 11$  at time 1 s.



(c) Snapshot of bluff body  $n = 11$  at time 2 s.



(d) Snapshot of bluff body  $n = 11$  at time 3 s.



(e) Snapshot of bluff body  $n = 11$  at time 4 s.



(f) Snapshot of bluff body  $n = 11$  at time 5 s.

## Snapshots of the Practical Run of Bluff Body $n = 12$



(a) Snapshot of bluff body  $n = 12$  at time 0 s.



(b) Snapshot of bluff body  $n = 12$  at time 1 s.



(c) Snapshot of bluff body  $n = 12$  at time 2 s.



(d) Snapshot of bluff body  $n = 12$  at time 3 s.



(e) Snapshot of bluff body  $n = 12$  at time 4 s.



(f) Snapshot of bluff body  $n = 12$  at time 5 s.